Glucocorticoid signaling is required for fatty acid β-oxidation (FAO) via transcriptional regulation of *carnitine palmitoyltransferase 1b* (*cpt1b*) in zebrafish

Yuqing Zhang[1,2], Shengchi Shi[1,2], Xi Li[4,*], Chuang Shi[1,2,3], Xinyi Wang[1,2], Jinli Xu[1,2], Qiyong Lou[1,2], Xia Jin[1], Jiangyan He[1], Zhan Yin[7,6,1,2,5], Gang Zhai[1,2,5,7,*]

[1]Key Laboratory of Breeding Biotechnology and Sustainable Aquaculture, Institute of Hydrobiology, Chinese Academy of Sciences, Wuhan, Hubei 430072, China

[2]College of Advanced Agricultural Sciences, University of Chinese Academy of Sciences, Beijing 100049, China

[3]School of Marine Biology and Fisheries, Collaborative Innovation Center of Nanfan and High-Efficiency Tropical Agriculture, Hainan Aquaculture Breeding Engineering Research Center, School of Breeding and Multiplication, Hainan University, Haikou 570228, China

[4]Center of Clinical Research, The Affiliated Kangning Hospital of Wenzhou Medical University, Wenzhou 325035, China

[5]Hubei Hongshan Laboratory, Huazhong Agriculture University, Wuhan, Hubei 430070, China

[6]Key Laboratory of Mariculture, Ministry of Education, Ocean University of China, Qingdao 266003, China

[7]Shenzhen Institute, Ocean University of China, Shenzhen, Guangdong 518100, China

*To whom correspondence should be addressed:

Xi Li

E-mail: xili_ihb@126.com

Gang Zhai

E-mail: zhaigang@ihb.ac.cn

Running title: Glucocorticoid is required for FAO

Uncorrected proof

ABSTRACT

Glucocorticoid (GC) signaling via glucocorticoid receptor (Gr) is crucial for vertebrate nutrient metabolism, but its regulatory role in lipid catabolism and the underlying the mechanism were still poorly understood. In this study, three hypocortisolism models of *proopiomelanocortin* (*pomca*)$^{-/-}$, *steroidogenic acute regulatory protein* (*star*)$^{-/-}$, *cyp17a2*$^{-/-}$ zebrafish, and one glucocorticoid resistance model of *gr*$^{-/-}$ zebrafish were used to investigate the role of GC signaling in lipid metabolism in vertebrates. Similar features of remodeled energy homeostasis, including accumulated fat deposition and enhanced glucose utilization, were observed in *star*$^{-/-}$, *cyp17a2*$^{-/-}$, and *gr*$^{-/-}$ zebrafish. Among the differentially expressed genes (DEGs) in liver, the *carnitine palmitoyltransferase 1b* (*cpt1b*) was identified as shared gene in *star*$^{-/-}$, *cyp17a2*$^{-/-}$, and *gr*$^{-/-}$ fish, compared to their respective control siblings. Administering hydrocortisone restored the decreased activity levels of fatty acid β-oxidation (FAO) activity and rescued the down-regulated hepatic and muscular expression of *cpt1b* in *star*$^{-/-}$, *cyp17a2*$^{-/-}$ fish, but not in *gr*$^{-/-}$ fish. Furthermore, we demonstrated that GC could activate *cpt1b* expression by acting on its proximal promoter region via Gr. However, when the fold changes were calculated across the four deficient models (relative to their respective control siblings), *pomca*$^{-/-}$ fish exhibited the greatest relative increase in testosterone level, but the least decrease in relative cortisol level and *cpt1b* expression. Consequently, unlike the other three fish models with impaired GC signaling, no adiposity was observed in *pomca*$^{-/-}$ fish. Overall, our results suggest that GC signaling enhances FAO by promoting *cpt1* expression, and the development of obesity due to impaired GC signaling depends on accompanying plasma steroid hormone profiles in fish.

Keywords: Glucocorticoid signaling; Fatty acid β-oxidation; *cpt1b*; Metabolism remodeling; Steroid profile

Uncorrected proof

INTRODUCTION

Hypocortisolism occurs when the body lacks sufficient cortisol, which is a steroid hormone produced by the adrenal glands. Cortisol plays an important role in the body's stress response, and metabolism, as well as in the regulation of blood pressure. The production of cortisol involves hypothalamic-pituitary-adrenal (HPA) axis in vertebrates or hypothalamic-pituitary-interrenal (HPI) axis in teleosts. This axis mainly includes corticotropin-releasing hormone (CRH) from the hypothalamus, and adrenocorticotropic hormone (ACTH), which is processed from Proopiomelanocortin (POMC) in the pituitary gland. It also includes many enzymes involved in the steroid synthesis pathway for cortisol production in the adrenal glands, and these form a molecular signal cascade in the form of a feedback loop that regulates cortisol levels. However, dysfunction at any point can lead to hypocortisolism (Krude et al., 1998; Sahakitrungruang et al., 2010; Shi et al., 2020).

Severe obesity associated with hypocortisolism has been reported in patients with variants of the POMC mutations and in POMC-deficient mice (Krude et al., 1998; Van Der Valk et al., 2022; Zemel & Shi, 2000). The obesity observed in mammals with POMC mutations has mainly been attributed to the altered regulation of melanocortin signaling derived from POMC on appetite (Krude et al., 1998; Raffan et al., 2016; Van Der Valk et al., 2022; Zemel & Shi, 2000). Ornithine has been reported as a metabolite related to the obesity of POMC mutant Labrador Retriever dogs (Söder et al., 2019). There is little information in previous literature on steroid hormones other than cortisol in organisms with *POMC* mutation-related hypocortisolism.

In the process of adrenal steroid synthesis, mutations in the *STAR* and *CYP21A2* genes have been identified as the causes of hypocortisolism (Caron et al., 1998; Ishii et al., 2002; Sahakitrungruang et al., 2010). Genetic depletion or loss-of-function mutations of *STAR* cause typical congenital lipoid hyperplasia (lipoid CAH), resulting in early death unless treated with cortisosteroids. The adrenal glands of patients and mice deficient in *STAR* exhibit disrupted cellular architecture and abundant lipid deposits. Their serum levels of adrenal steroid hormones, including corticosterone and testosterone, were low in the early stages (Caron et al., 1998; Ishii et al., 2002; Sahakitrungruang et al., 2010). Since adult *STAR* mutants depend on chronic administration of exogenous corticosteroids, the obesity phenotype due to their intrinsic hypocortisolism was unobservable. Over 95% of CAH cases are caused by a variety of polymorphisms in *CYP21A2* in patients. *CYP21A2* deficiency normally leads to excessive

androgen production and diminished cortisol synthesis (Kara et al., 2024). Glucocorticoid (GC) replacement therapy is usually necessary for survival in CAH. Therefore, the treatment course could potentially interfere with the assessment of clinical syndrome features (Falhammar et al., 2015). However, overweight, obesity, or increased abdominal adiposity were more frequently observed in *CYP21A2*-deficient patients than in controls (Bacila et al., 2022; Kim et al., 2015). Although murine and human *CYP21A2* show a high level of homology (77.5% DNA identity and 72.5% protein identity), it would still be difficult to perform a functional analysis on many types of polymorphism identified in humans using mouse models. Furthermore, *CYP21A2*-deficient mice die at an early postnatal stage. Despite intensive dexamethasone treatment, the mouse model remains difficult to use in studies (Schubert et al., 2022). To elucidate the relationship between nutrient metabolism and CAH due to *21-hydroxylase* deficiency, a *cyp21a2*-deficient zebrafish model was generated recently. This model exhibited CAH and hypocortisolism, as well as increased body weight and fat deposition. It was also demonstrated that several biological processes involved in lipid metabolism and ATP synthesis were dysregulated in *cyp21a2*-deficient zebrafish. Unlike *cyp21a2*-deficient mammals, hyperandrogenism was not observed in *cyp21a2*-deficient zebrafish (Bacila et al., 2025).

In the mammalian HPA axis, mutations in the nuclear *glucocorticoid receptor* (*GR*) can impair cortisol signaling *in vivo*. Depending on their functional type, *GR* mutations can be classified as either gain-of-function or loss-of-function. Depletion of *GR* or loss of function of GR genes typically causes GC resistance in mutants. In terms of the functioning of GC signaling, GR deficiency mimic certain effects of hypocortisolism *in vivo*. Defects associated with loss-of-function *GR* mutations have been reported to include neonatal hypoglycaemia, severe dehydration and high blood pressure. ACTH overstimulation of the adrenal gland accounts for increased levels of circulating glucocorticoids, androgens and cortisol. Some patients exhibit increasing visceral obesity (Vitellius et al., 2018). Due to the absence of aldosterone in teleosts, glucocorticoids can function dually as glucocorticoids and mineralocorticoids, exerting their impacts through interaction with GR or mineralocorticoid receptor (MR)(Guh et al., 2015). In modulating lipid metabolism, the two glucocorticoid receptors serve distinct functions, with MR activation enhancing lipid synthesis and GR activation stimulating lipid breakdown (Faught & Vijayan, 2019b). Despite this, the mechanism involved in GR-mediated lipid catabolism is still unknown.

Congenital hypocortisolism has been found to be caused by various gene mutations, including those of the POMC, STAR and CYP21A2 genes. These mutations have also been associated with different levels of obesity (Bacila et al., 2022; Bacila et al., 2025; Kim et al., 2015; Krude et al., 1998; Raffan et al., 2016; Van Der Valk et al., 2022; Vitellius et al., 2018; Zemel & Shi, 2000). However, it is difficult to explore the mechanism connecting deduced cortisol with lipid metabolism due to the variety of gene polymorphisms and the complications caused by medication administered to patients. Furthermore, the presence of species-specific HPA features, even between humans and mice, often hinders successful studies using individual animal models (Schubert et al., 2022). A systematic investigation using a series of animal models could help to unravel the complexity of adrenal steroid synthesis regulatory networks.

The synthesis of GC predominantly takes place in the interrenal gland of teleosts, where it is regulated by the hypothalamic–pituitary–interrenal (HPI) axis, as in the HPA axis of mammals (Dinarello et al., 2020). The zebrafish is becoming a popular model for investigating the synthesis of steroid hormones, including estradiol, testosterone, progesterone and cortisol (the main glucocorticoid in zebrafish)(Eachus et al., 2017; Lau et al., 2016; Ruan et al., 2024; Yin et al., 2017; Zhai et al., 2018; Zhai et al., 2022; Zhang et al., 2020). Recently, *star*$^{-/-}$ and *cyp17a2*$^{-/-}$ zebrafish were generated in this laboratory and exhibited hypocortisolism (Shang et al., 2019; Shi et al., 2022). Additionally, *gr*$^{-/-}$ zebrafish have been generated in this laboratory for this study to model GC resistance. Most *star*$^{-/-}$, *cyp17a2*$^{-/-}$ and *gr*$^{-/-}$ zebrafish survive to adulthood without any exogenous corticosteroid therapy.

It was reported that MR is a key modulator of glucose metabolism in the musculature of zebrafish during basal and stress conditions (Faught & Vijayan, 2022). In this study, *star*$^{-/-}$, *cyp17a2*$^{-/-}$, and *gr*$^{-/-}$ zebrafish were set out to investigate the regulatory role of GC/Gr signaling in lipid metabolism, which constitute valuable models for the systematic comparative analysis of GC signaling functions in metabolism and growth in fish. All our three mutants exhibited obesity with impaired GC signaling. Furthermore, energy homeostasis remodeling is mediated by compromised FAO in zebrafish coincided with the phenotype of zebrafish with the *cpt1b* mutation, which was found to be transcriptionally regulated by glucocorticoid signaling in this study. Our comparative analyses of adrenal hormone profiles in our series of mutants suggest that the obesity-like phenotypes observed in fish with hypocortisolism may depend on the context steroid profiles.

MATERIALS AND METHODS

Zebrafish maintenance

The zebrafish were maintained as previously described (Westerfield, 2020). Briefly, they were reared at 28±2℃ under a 14-hour light and 10-hour dark cycle in a recirculating water system. After hatching, zebrafish larvae were initially fed with egg yolk suspension for 7 days, then transitioned to twice-daily feedings of newly hatched brine shrimp. Approximately 80 fish were kept in a 10 L tank. All experimental zebrafish in this study were maintained until 4 months post-fertilization (mpf). In light of the need to minimize the impact of physiological variability associated with sex differences and cyclical hormonal fluctuations in females, male fish were randomly selected for the analyses according to previous studies (Li et al., 2020a; Wang et al., 2024; Xi et al., 2023). All animal experiments were conducted in accordance with the Guiding Principles for the Care and Use of Laboratory Animals and were approved by the Institute of Hydrobiology, Chinese Academy of Sciences (Approval ID: IHB 202458ZY).

Gene knockout

We obtained a knockout line with a 1 bp deletion in the second exon of *star* by utilizing transcription activator-like effector nucleases (TALENs) that target the left arm recognition sequence (5'–AGCACTTGGATAAACCACAT–3') and the right arm recognition sequence (5'–AGTAAGAGATCTTGCAT–3') (Shang et al., 2019). The *cyp17a2* knockout zebrafish line, carrying a 7 bp deletion in the second exon, was generated with the CRISPR/Cas9 strategy. The specific guide RNA (gRNA) targeting site on the genomic DNA adjacent to the NGG of Protospacer Adjacent Motif (PAM) region is GGGGCAGAGAGTTCGCCGGA (Shi et al., 2022). The *gr* knockout zebrafish line, carrying a 7 bp deletion in the first exon, was generated with the CRISPR/Cas9 strategy. The specific gRNA targeting site on the genomic DNA adjacent to the PAM region is GGCCCTGCAACAGCAGACCT. The primers used for genotype examination were provided in Supplementary Table S1.

Growth performance

Zebrafish at 4 mpf were randomly selected, anesthetized with MS-222, and then their body length and the corresponding weight were measured and recorded. BMI was calculated by dividing body weight (g) by the square of body length (cm).

Whole-mount *in situ* hybridization (WISH)

WISH in zebrafish was performed as previously described (Thisse & Thisse, 2008) with

Uncorrected proof

modifications. Larvae at 5 days post-fertilization (dpf) were fixed in 4% paraformaldehyde (PFA) overnight at 4°C, and then permeabilized with proteinase K treatment (10 μg/mL). After prehybridization, samples were incubated with digoxigenin-labeled RNA probes at 65°C for 16 hours. Antisense probes were made from the cDNA of *proopiomelanocortin a* (*pomca*), *cytochrome P450, family 11, subfamily A, polypeptide 1* (*cyp11a1*), and *cytochrome P450*, *family 21*, *subfamily A*, *member 2* (*cyp21a2*). Post-hybridization washes were performed sequentially with gradually diluted saline sodium citrate. After blocking with 2% bovine serum albumin (BSA), anti-DIG-AP antibody (11093274910, Roche, Switzerland) was applied overnight at 4°C. Color development was achieved using NBT/BCIP Stock Solution (11681451001, Roche, Switzerland) in the dark at room temperature. The reaction was terminated with phosphate buffered saline with tween 20 (PBST) washes, and samples were post-fixed in 4% PFA for long-term preservation. Imaging was conducted using an Olympus microscope (Olympus, Japan). The pixel values of WISH signals were measured and quantified using National Institute of Health (NIH) ImageJ analysis software.

Analysis of visual background adaptation (VBA)

The illumination-induced pigment dispersion assay was used for the analysis of VBA in zebrafish as previously described (Li et al., 2020b). Firstly, the zebrafish larvae at 4 dpf were maintained in a dark environment for a minimum of 60 min, after which they were exposed to bright illumination for 30 min. The larvae were then anesthetized with MS-222 and fixed with 4% PFA/phosphate buffered saline (PBS). Subsequently, images were captured using an Olympus microscope (Olympus, Japan). The region of interest (ROI) on the larval head was defined, and the area of melanin within the ROI was quantified using NIH ImageJ analysis software (Zhang et al., 2022).

Zebrafish behavioral analysis

Zebrafish at 4 mpf were analyzed for the movement distance every 30 s within 20 min under the alternating 5 min intervals of light and dark. The behavior was monitored using a ZebraTower system (ViewPoint Life Sciences, Canada). More than twelve fish of each genotype were used as replicates.

Total RNA isolation and quantitative real-time polymerase chain reaction (qPCR)

The liver and muscle of zebrafish at 4 mpf were homogenized using TRIzol reagent (Cat. 15596-018, Invitrogen, USA) to isolate the total RNA. After purification, 1 μg of the RNA

Uncorrected proof

template was subjected to reverse transcription using the EasyScript One-Step gDNA Removal and cDNA Synthesis Super Mix Kit (Cat. AE311-03, Beijing TransGen Biotech, China) to generate complementary DNA (cDNA). The qPCR assays were performed using the PerfectStart™ Green qPCR Super Mix Kit (Cat. AQ601-02-V2, Beijing Transgen, China) on a CFX Connect Real-Time PCR Detection System (Bio-Rad, USA). Data quantification was performed following the $2^{-\Delta\Delta Ct}$ method outlined in previous research (Livak & Schmittgen, 2001). Details of the primer sequences for *acyl-CoA oxidase 3, pristanoyl* (*acox3*), *carnitine palmitoyltransferase 1aa* (*cpt1aa*), *cpt1ab*, *cpt1b*, *cpt2*, *peroxisome proliferator-activated receptor alpha a* (*pparaa*), *pparab*, and *β-actin* used in the present study were provided in Supplementary Table S1.

Triglyceride (TG) and non-esterified free fatty acids (NEFA) measurements, and lipid content quantification

The TG and NEFA levels in the liver, muscle, visceral mass, and plasma of zebrafish at 4 mpf were assayed using the Triglyceride Assay Kit (Cat. A110-1-1, Nanjing Jiancheng Bioengineering Institute Co., Ltd., China) and the Free Fatty Acid Content Assay Kit (Cat. A110-1-1, Grace Biotechnology Co., Ltd., China), following the manufacturer's instructions. All measurements were performed in biological duplicates and technical triplicates. Total lipid content in whole zebrafish was measured using the Folch method (Folch et al., 1957). Briefly, euthanized fish were rinsed with PBS, blotted dry, and lyophilized. The dried samples were homogenized, and the lipids were extracted using the Folch method with chloroform-methanol solvent (2:1 v/v). After centrifugation, the organic phase was collected and the solvents were evaporated under nitrogen, and the lipid residue were weighed. Total lipid percentage was calculated as (lipid mass / dry sample mass) × 100.

Micro-computed tomography (micro-CT) imaging and Nile Red staining

Images of zebrafish adipose tissue were obtained using the micro-CT system (SkyScan 1276, Germany). The fish were anesthetized and scanned at high resolution to produce three-dimensional (3D) volumetric images. The adipose tissue was segmented based on density thresholds, and the volume of fat deposits was quantified using Skyscan CTAn software (v.1.1.7, Skyscan CTAn, Belgium). Based on the previous report (Peng et al., 2017), neutral lipid staining was conducted with Nile Red dye (N3013, Sigma, USA) at a working concentration of 0.1 μg/mL in the dark for overnight. Images were then obtained using an Olympus SZX16FL

Uncorrected proof

stereomicroscope (Olympus, Japan) at an excitation wavelength of 488 nm.

Enzyme activity measurements

The activity of Cpt1 in the liver and muscle was assayed using the commercial kit (Cat. QYS-239012) purchased from Qiyi Biological Technology Co., Ltd. (China), according to the manufacturer's instructions. The activity of the enzymes glucokinase (Gck), phosphofructokinase (Pfk) and pyruvatekinase (Pk) in the liver and muscle was measured according to the manufacturer's instructions from Suzhou Grace Biotechnology Co., Ltd. (China). All measurements were performed in biological triplicates and technical duplicates.

Plasma cortisol and testosterone concentrations analyses

The concentrations of cortisol and testosterone in plasma of zebrafish at 4 mpf were examined using Cortisol enzyme linked immunosorbent assay (ELISA) Kit (Cayman Chemical, 500360, USA) and Testosterone ELISA Kit (Cayman Chemical, 582701, USA) (Shi et al., 2020; Shi et al., 2025; Zhai et al., 2018). Briefly, the total steroids were extracted from 10 μL plasma using a mixture of n-hexane and ethyl acetate (1:1 v/v). Following vortex and centrifugal separation, the organic layer was transferred to a fresh tube and extracted three times repeatedly. The organic part was evaporated by heating to 37°C under a gentle and slow flow of nitrogen. Finally, the extract was dissolved in 500 μL ELISA buffer and prepared for measurement according to the manufacturer's instructions.

Fatty acid β-oxidation (FAO) rates measurement

The FAO rates of liver and muscle were quantified using the Fatty Acid Oxidation Assay Kit (Cat.BR00001) from Assay Genie (Ireland) following the manufacturer's instructions. All measurements were performed in biological triplicates and technical duplicates.

Metabolite extraction and metabolomic analysis

Frozen samples stored at –80°C were thawed on ice and homogenized using a grinder (30 Hz, 20 s), then centrifuged at 3000×g for 30 s at 4°C. A 400 μL solution (methanol:water=7:3, v/v) containing an internal standard was added in to 20 mg grinded sample, and vortexed at 2500×g for 5 min. After incubation on ice for 15 min, the sample was centrifuged at 12000×g for 10 min at 4°C. The 300 μL collected supernatant placed in –20°C for 30 min, then centrifuged again. Finally, 200 μL aliquots of the supernatant were transferred for LC-MS analysis. The sample extracts were analyzed using an LC-ESI-MS/MS system. After normalization and quality control filtering of raw data, differential metabolites were identified through multivariate

Uncorrected proof

statistical analysis. Differential metabolites were determined by Variable importance in projection (VIP) (>1) and *P* value (<0.05).

RNA-seq and analysis

Total RNA was isolated from the liver using Trizol Reagent (Invitrogen Life Technologies, USA). The concentration, quality and integrity were then determined using a NanoDrop spectrophotometer (Thermo Scientific, USA). The sequencing library was constructed using the NEBNext Ultra II RNA Library Prep Kit (New England Biolabs Inc, USA) for Illumina Kit and then sequenced on the NovaSeq 6000 platform (Illumina, USA). The filtered reads were mapped to the *Danio rerio* genome (GRCz11) using HISAT2 (v.2.1.0). FASTP (v.0.22.0) software was used to filter the sequencing data to get high quality sequence (clean data) for further analysis. HTSeq (v.0.9.1) statistics were used for expression analysis to compare the read count for each gene with the original gene expression, and then FPKM was used to standardize the expression. The differential expression gene analysis was performed using DESeq (v.1.38.3), filtering according to the following conditions: the fold change in expression $|\log_2 \text{fold change}|>2$, and the significance *P*-value<0.05.

Hydrocortisone (HC) administration

The HC was purchased from Sigma Aldrich (Cat.H1885, USA) and dissolved in dimethyl sulfoxide (DMSO) at the stocking concentration of 60 mg/mL. Chemical exposure was conducted by immersing the fish in water containing HC. WT male zebrafish were treated with HC at 0.005, 0.05, 0.5 and 5 mg/L for qPCR analysis for 24 hours. The *star*-, *cyp17a2*-, and *gr*-depleted zebrafish were treated with HC at 5 mg/L for 24 hours for qPCR analysis and 12 days (the medium containing HC was refreshed every 3 days) for the enzyme activity measurement of Cpt1. The concentration and duration of administration were selected according to previous studies (Faught & Vijayan, 2019b; Nipu et al., 2022) .

Dual-Luciferase reporter assay

Using high-fidelity PCR technology, the full-length open reading frame (ORF) of the *gr* cDNA and the promoter region of the *cpt1b* gene were amplified. Details of the primer sequences used to amplify the full-length Gr ORF and the *cpt1b* promoter are provided in Supplementary Table S1. Following double restriction digestion and purification, the Gr ORF fragment was directionally inserted into the pCMV vector via homologous recombination, while the *cpt1b* promoter fragment was inserted into the pGL3-Basic vector. The ligation products

Uncorrected proof

were transformed into *E. coli* DH5α competent cells. Positive recombinant plasmids were confirmed by colony PCR and Sanger sequencing. Human embryonic kidney cells (HEK 293T) were used for the dual-luciferase reporter assay. HEK 293T cells were maintained in high glucose Dulbecco's modified eagle medium (DMEM, Cat. 11965092, Thermo Fisher Scientific, USA), supplemented with 10% fetal bovine serum (FBS, Cat. 04-001-1ACS, Biological Industries, Israel), and grown at 37°C in a humidified incubator with 5% CO_2. When the HEK 293T cells in the 24-well plates reached approximately 70-80% confluence, the indicated plasmids were transfected into the cells using transfection reagents, and incubation continued for 12 hours. The original medium was then replaced with serum-free DMEM containing 10 pM–10 μM HC, and incubation was continued at 37°C for 12 hours. Subsequently, the cells were washed with PBS and collected for measuring firefly luciferase and Renilla luciferase activities using the Dual-Luciferase Reporter Assay System (Cat. E1910, Promega, USA) and a Sirius Luminometer (Berthold Detection Systems). Firefly luciferase activity was normalized against Renilla luciferase data, and the induction factor was calculated by dividing the average luciferase activity in the steroid-exposed experimental groups by the corresponding measurement in the control groups maintained without steroid treatment.

Blood glucose and dynamic detection

The blood glucose levels in zebrafish at 4 mpf were measured using the OneTouch UltraVue (LifeScan, Inc., USA) glucometer at 0, 1, and 2 h after feeding. Fasting zebrafish at 4 mpf were immersed in a 3% glucose solution for 3 h, and blood glucose concentrations were measured at 30, 60, 90, and 120 min after the induction of hyperglycemia.

Statistical analysis

Statistical analyses were performed using GraphPad Prism 8.0 (GraphPad Software, San Diego, CA, USA). We first performed normality testing (Shapiro-Wilk test) and homogeneity of variance testing (Levene's test). When data met the criteria of normal distribution and equal variance, Student's *t*-test or one-way ANOVA with Tukey's multiple comparisons were used to analyze intergroup differences. All results are presented as mean±standard deviation (SD). For all statistical analyses, $P<0.05$ indicated a significant difference, with significance set to: *, $P<0.05$. **, $P<0.01$. ***, $P<0.001$. ****, $P<0.0001$.

Uncorrected proof

RESULTS

star-depletion resulted in inactivated pituitary-interrenal axis

Intercrossing *star*$^{+/-}$ males and females generated offspring with *star*$^{+/+}$, *star*$^{+/-}$ and *star*$^{-/-}$ genotypes in a Mendelian inheritance ratio of 1:2:1. From WISH analyses using the probes of *pomca*, *cyp21a2* and *cyp11a1*, significantly up-regulated expression levels of pituitary *pomca* and interrenal gland *cyp11a1* and *cyp21a2* in *star*-deficient fish at 5 dpf was observed (Figure 1A–G). These results demonstrate that *star* depletion simultaneously up-regulates *pomca* in the pituitary and steroidogenic genes (*cyp11a1*, *cyp21a2*) in the interrenal gland, indicating a loss of the negative feedback in the pituitary-interrenal axis caused by impaired steroidogenesis.

The light-stimulated stress response in the *star*$^{-/-}$ fish at 4 mpf was also significantly down-regulated, as evidenced by the distance statistically analyzed in every 30 seconds and in total (Figure 1H, I). The decreased oxygen consumption was observed in *star*$^{-/-}$ fish (Figure 1J). The analysis of VBA demonstrated that the *star*$^{-/-}$ fish exhibited disrupted light-induced melanosome condensation, as the pigmented areas in the ROI were significantly larger than those in *star*$^{+/+}$ fish of control siblings (Figure 1K–M). These results suggested that *star* depletion resulted in inactive pituitary-interrenal axis, which could be supported by the decreased cortisol concentrations in *star*$^{-/-}$ zebrafish (Figure 1N).

star-deficient zebrafish exhibited excessive lipid content in various tissues

Compared to *star*$^{+/+}$ fish, the *star*$^{-/-}$ fish showed increased body weight and body mass index (Figure 2A, B). Whole-body lipid images using micro-CT revealed greater visceral adipose tissue (VAT) accumulation in *star*$^{-/-}$ fish than in *star*$^{+/+}$ fish of control siblings (Figure 2C–E). Total lipid content and plasma triglyceride levels were significantly increased in *star*$^{-/-}$ fish compared to *star*$^{+/+}$ fish (Figure 2F, G). Comparative analysis of total lipid content was also conducted in body weight-matched *star*$^{+/+}$ (0.3144±0.01670 g) and *star*$^{-/-}$ (0.3168±0.03239 g) individuals, revealing that lipid content was significantly higher in *star*$^{-/-}$ fish than in body weight-matched *star*$^{+/+}$ fish (13.80±1.755% vs. 18.02±3.520%, respectively) (Supplementary Table S2). Meanwhile, the concentrations of triglycerides in visceral mass and muscle, and non-esterified fatty acids in liver were increased in *star*$^{-/-}$ fish compared to *star*$^{+/+}$ fish (Figure 2H, I).

Cpt1 is the rate-limiting enzyme in catalyzing mitochondrial β-oxidation. To determine the mechanism related to elevated lipid content in *star*$^{-/-}$ fish, the expression of the genes related to FAO was assessed using qPCR. It was observed that the FAO-related genes were significantly

Uncorrected proof

down-regulated in the liver and muscle of *star*$^{-/-}$ fish, including *acox3*, *cpt1aa*, *cpt1ab*, *cpt1b*, *cpt2*, *pparaa* and *pparab* (Figure 3A, B). Furthermore, the enzyme activity and FAO activities of Cpt1 were significantly decreased in the liver and muscle of *star*$^{-/-}$ fish (Figure 3C, D). Cpt1 promotes the conversion of long-chain fatty acyl CoA ligands and carnitine into acyl carnitine (Lopes et al., 2022). Notably, the contents of acyl carnitine were significantly decreased in *star*$^{-/-}$ fish compared to *star*$^{+/+}$ fish (Figure 3E).

star-deficient zebrafish exhibited improved glucose utilization and increased protein deposition

We then examined the glucose dynamics in the *star*$^{+/+}$ and *star*$^{-/-}$ zebrafish at different time points after feeding. The *star*$^{-/-}$ fish demonstrated hypoglycemia during fasting and after food intake, as evidenced by the blood glucose measurements taken at 0, 1 and 2 h after feeding (Figure 4A–C). The curve of glucose dynamics analysis demonstrated that the blood glucose of *star*$^{-/-}$ fish was consistently lower than that of *star*$^{+/+}$ fish. A statistically significant difference was observed 3 hours before and 90 and 120 min after 3% glucose solution administration. No statistically significant difference was observed in the comparison between *star*$^{+/+}$ and *star*$^{-/-}$ fish at 30 and 60 min after 3% glucose solution administration, suggesting that the *star*$^{-/-}$ fish exhibited faster glucose clearance (Figure 4D). The activity of the key glycolytic pathway enzymes, glucokinase (Gck) and phosphofructokinase (Pfk), was significantly increased in the liver and muscle of *star*$^{-/-}$ fish (Figure 4E, F). However, the enzyme activity of pyruvate kinase (Pk) in the liver and muscle was comparable between *star*$^{-/-}$ fish and *star*$^{+/+}$ fish (Figure 4G). These results suggested that *star*$^{-/-}$ fish exhibited FAO-inhibition but enhanced glycolysis.

The protein content was higher in the *star*-deficient fish (Figure 4H). Comparative analysis of crude protein content was also conducted in body weight-matched *star*$^{+/+}$ (0.2473±0.01729 g) and *star*$^{-/-}$ (0.2640±0.01149 g) individuals, revealing that the protein content was significantly higher in *star*$^{-/-}$ fish than in body weight-matched *star*$^{+/+}$ fish (55.99±2.578% vs. 59.80±2.601%, respectively) (Supplementary Table S3).

HC treatment rescued *cpt1* and *cpt2* expression in *star*$^{-/-}$ fish

Subsequently, HC at different concentrations was administered to the WT fish. The results showed that HC administration in WT fish elevated the expression of *cpt1b* both in liver and muscle in a dose-dependent manner (Supplementary Figure 1A, B). HC at 5 mg/L was then administered to *star*$^{+/+}$ and *star*$^{-/-}$ fish. The results showed that HC administration in *star*$^{+/+}$ fish

Uncorrected proof

elevated the expression of *cpt1aa*, *cpt1b* and *cpt2* in liver (Figure 5A, Tangerine). Furthermore, the down-regulated expression of *cpt1aa*, *cpt1ab*, *cpt1b*, and *cpt2* in the liver of *star*$^{-/-}$ fish (Figure 5A, Yellow) could be effectively rescued following HC treatment (Figure 5A, Green). Furthermore, HC administration in *star*$^{+/+}$ fish also increased the expression of *cpt1ab*, *cpt1b* and *cpt2* in muscle (Figure 5B, Tangerine), while the down-regulated expression of *cpt1aa*, *cpt1ab*, *cpt1b* and *cpt2* in the muscle of *star*$^{-/-}$ fish (Figure 5B, Yellow) was similarly rescued after HC treatment (Figure 5B, Green). These results suggested that the cortisol levels were positively correlated with the expression of *cpt1*.

Furthermore, the enzyme activity of Cpt1 was significantly increased in the liver of HC-treated fish (Figure 5C). The decreased Cpt1 activity in the liver and muscle of *star*$^{-/-}$ fish could be effectively rescued following HC treatment (Figure 5C, D). These results indicated that cortisol levels were positively correlated with the enzyme activity of Cpt1.

***cyp17a2*- and *gr*-deficient fish both exhibited excessive lipid content**

Similar to *star*-deficient zebrafish, *cyp17a2*-deficient zebrafish also exhibited impaired cortisol synthesis (Shi et al., 2022), while *gr*-deficient zebrafish represented a model of cortisol resistance. We then set out to integrate these three models for a comprehensive dissection of glucocorticoid-mediated regulation of lipid metabolism. Compared to their male control siblings, the *cyp17a2*$^{-/-}$ fish exhibited decreased cortisol concentration, which was increased in *gr*$^{-/-}$ fish (Figure 6A, M). Meanwhile, the *cyp17a2*$^{-/-}$ and *gr*$^{-/-}$ fish also exhibited increased body weight and body mass index compared to their control siblings (Figure 6B, C, J, K). The expansion of VAT was also observed in *cyp17a2*$^{-/-}$ and *gr*$^{-/-}$ fish compared to the size-matched control siblings through Nile Red staining (Figures 6D, L). Total lipid content was significantly increased in *cyp17a2*$^{-/-}$ and *gr*$^{-/-}$ fish (Figure 6E, M), whereas blood glucose was significantly decreased in *cyp17a2*$^{-/-}$ and *gr*$^{-/-}$ fish compared to their control siblings (Figure 6F, N). HC was then administered to the male *cyp17a2*$^{-/-}$ and *gr*$^{-/-}$ fish. HC administration in *cyp17a2*$^{+/+}$ and *gr*$^{+/+}$ fish of their control siblings elevated the expression of *cpt1b* in liver and muscle (Figure 6G, H, O, P, lane 2 vs lane 1). The down-regulated *cpt1b* in the liver and muscle of *cyp17a2*$^{-/-}$ fish (Figure 6G and H, lane 3 vs lane 1) could be effectively rescued following HC treatment (Figure 6G, H, lane 4 vs lane 1). However, the down-regulation of *cpt1b* in the liver and muscle of *gr*$^{-/-}$ fish (Figure 6O, P, lane 3 vs lane 1) could not be effectively rescued by HC treatment (Figure 6O, P, lane 4 vs lane 3). These results confirmed that GC positively regulated the expression of *cpt1*

Uncorrected proof

via Gr.

Glucocorticoid signaling regulates the expression of *cpt1b* in zebrafish

To characterize the intersected genes that were differentially expressed, the differentially expressed genes (DEGs) from the transcriptome comparisons of the liver of *star*$^{-/-}$, *cyp17a2*$^{-/-}$ and *gr*$^{-/-}$ fish and their control siblings, were analyzed integratively. A total of 52 DEGs in the intersected region were obtained in liver of *star*$^{-/-}$, *cyp17a2*$^{-/-}$ and *gr*$^{-/-}$ fish (Figure 7A), among which, 11 and 41 genes were up- and down-regulated respectively (Supplementary Table 4). Among the down-regulated genes, the *cpt1b* was simultaneously observed in the liver of *star*$^{-/-}$, *cyp17a2*$^{-/-}$ and *gr*$^{-/-}$ fish (Figure 7B). This suggests that the glucocorticoid signaling pathway may positively regulate the expression of *cpt1b*, which was down-regulated, causing inhibited FAO and enhanced lipid content in *star*$^{-/-}$, *cyp17a2*$^{-/-}$, and *gr*$^{-/-}$ fish.

To determine whether the *cpt1b* promoter could be activated by GC via Gr, the expression vector of pCMV-Gr and *cpt1b* promoter luciferase reporter plasmid were transfected into HEK 293T cells, which were then treated with HC. The result of relative luciferase activity demonstrated that when simultaneously transfected with the expression vector of Gr, *cpt1b* promoter could be gradually activated by the HC administration in a dose-dependent manner; however, this activation effect was not observed in the absence of Gr (Figure 7C). We also performed a series of deletions on the *cpt1b* promoter that drives the luciferase reporters. Among the constructions, the deletion of 734-1306 bp promoter region led to significantly decreased relative luciferase activity, among which, the deletion of 924-1020 bp promoter region led to significantly decreased relative luciferase activity compared to the other deletions (Figure 7D).

The relatively highest plasma cortisol and testosterone levels and the least down-regulated hepatic *cpt1b* expression in *pomca*-deficient zebrafish

POMC is a key pituitary regulator of HPI axis regulates essential physiological adaptations to stress in teleosts (Gonzalez-Nunez et al., 2003). The down-regulation of *cpt1b* was also observed in liver and muscle of *pomca*$^{-/-}$ fish, which was a hypocortisolism model as well (Figure 8A). To explore the *pomca*$^{-/-}$ fish without increasing adiposity in contrast to the *star*$^{-/-}$, *cyp17a2*$^{-/-}$ and *gr*$^{-/-}$ fish at 4 mpf, the cortisol and testosterone concentrations in the plasma were compared systemically. For cortisol, the *pomca*$^{-/-}$ fish, which did not exhibit adiposity (Shi et al., 2020), showed the least decrease compared to the *star*$^{-/-}$ and *cyp17a2*$^{-/-}$ fish when calculated to the ratio compared to their control siblings (0.0098 for *star*$^{-/-}$ fish and 0.0154 for *cyp17a2*$^{-/-}$ fish

Uncorrected proof

but 0.0692 for *pomca*$^{-/-}$ fish) (Table 1).

Correspondingly, *pomca*$^{-/-}$ fish also exhibited the relatively least decreased levels of the hepatic *cpt1b* expression compared to those of the *star*$^{-/-}$, *cyp17a2*$^{-/-}$ and *gr*$^{-/-}$ fish when calculated to the ratio compared to their control siblings (0.0085 for *star*-deficient fish, 0.1984 for *cyp17a2*$^{-/-}$ fish, 0.1390 for *gr*$^{-/-}$ fish but 0.3549 for *pomca*$^{-/-}$ fish) (Table 1). On the other hand, for testosterone, the *pomca*$^{-/-}$ fish showed the relatively greatest increased levels compared to those of *star*$^{-/-}$ and *cyp17a2*$^{-/-}$ fish, as calculated to the ratio compared to their control siblings (1.248 for *star*-deficient fish, 2.260 for *cyp17a2*$^{-/-}$ fish but 4.174 for *pomca*$^{-/-}$ fish) (Table 1).

The *hydroxyl-delta-5-steroid dehydrogenase-3β-and steroid delta-isomerase 1* (*hsd3b1*) encodes the key enzyme responsible for cortisol synthesis, while the *17β-hydroxysteroid dehydrogenase type 3* (*hsd17b3*) encodes the enzyme responsible for final conversion of androstenedione into testosterone. Decreased *hsd3b1* and increased *hsd17b3* were observed in *pomca*$^{-/-}$ zebrafish. This was hypothesized to result in skewed cortisol synthesis towards testosterone (Shi et al., 2020). The *cyp11a1*, *cyp11c1*, *cyp17a1*, *cyp19a1a*, *cyp21a1*, *hsd17b3* and *hsd3b1* of key genes involved in steroidogenesis were examined in interrenal gland of *star*$^{-/-}$, *cyp17a2*$^{-/-}$ and *gr*$^{-/-}$ fish and their control siblings. Most of interest, *cyp11a1*, *cyp11c1*, *cyp19a1a* and *cyp21a1* were up-regulated in *star*$^{-/-}$, *cyp17a2*$^{-/-}$ and *gr*$^{-/-}$ fish compared to their control siblings. Meanwhile, *cyp17a1* were up-regulated in *cyp17a2*$^{-/-}$ and *gr*$^{-/-}$ fish compared to their control siblings. However, unlike *pomca*-deficient zebrafish, the expression of *hsd17b3* was comparable, while *hsd3b1* was found to be up-regulated in the comparison between *star*-, *cyp17a2*$^{-/-}$ and *gr*$^{-/-}$ fish and their control siblings (Figure 8B–D). These results suggested that the skewed cortisol synthesis towards testosterone due to decreased *hsd3b1* and increased *hsd17b3* were observed only in *pomca*$^{-/-}$ fish, not in *star*$^{-/-}$, *cyp17a2*$^{-/-}$ and *gr*$^{-/-}$ fish.

Uncorrected proof

DISCUSSION

This study utilized compromised GC/Gr signaling models of *pomca*$^{-/-}$, *star*$^{-/-}$, *cyp17a2*$^{-/-}$ and *gr*$^{-/-}$ zebrafish for systematic comparative analyses. These models exhibited various levels of lipid accumulation and reduced mitochondrial fatty acid oxidation (FAO) activity, but increased glucose utilization capacity. Decreased levels of hepatic and muscular *cpt1b* expression were observed in all four impaired GC/Gr signaling zebrafish models. These results indicate that down-regulation of *cpt1b* expression via GC/Gr signaling could be attributed to a key regulator of FAO.

The TALENs, CRISPR/Cas9 and morpholino methods were used for the knockout or knockdown of *star*, *cyp17a2*, *cyp11a1*, *cyp11a2* and *hsd3b1*. The mutants or morphants were found to be cortisol deficient, as evidenced by this study and others (Eachus et al., 2017; Li et al., 2020a; Lin et al., 2015; Parajes et al., 2013; Shang et al., 2019; Shi et al., 2022). As observed in *cyp17a2*$^{-/-}$ zebrafish, an enlarged interrenal gland accompanied by up-regulation of *pomca* in the pituitary was observed in these mutants or morphants (Eachus et al., 2017; Li et al., 2020b; Lin et al., 2015; Parajes et al., 2013; Shang et al., 2019; Shi et al., 2022). We recently observed that *pomca*$^{-/-}$ zebrafish exhibited decreased locomotion activity and oxygen consumption (Shi et al., 2020). Similarly impaired locomotion activity and response to light-stimulated stress, as well as decreased oxygen consumption, were observed in *cyp17a2*$^{-/-}$ and *star*$^{-/-}$ fish at the adult stage. This confirms that *cyp17a2*$^{-/-}$ and *star*$^{-/-}$ fish are a model of stress response blunting and hypocortisolism. An increased body weight phenotype was observed in *star*$^{-/-}$, *cyp17a2*$^{-/-}$, and *gr*$^{-/-}$ zebrafish. Unlike *pomca*$^{-/-}$ fish, which did not show increased lipid accumulation as previously reported (Shi et al., 2020), this study first demonstrated that *star*$^{-/-}$, *cyp17a2*$^{-/-}$, and *gr*$^{-/-}$ fish all exhibited significantly higher lipid content compared to their age-matched control siblings. This was also observed when comparing body weight-matched control siblings and mutants. These results suggest that the higher lipid content in the mutants may be caused by impaired GC/Gr signaling directly rather than by changed locomotor activity indirectly.

The GC/Gr complex modulates gene expression by binding directly to DNA or to other DNA-bound transcription factors, or to both simultaneously, thereby stimulating or repressing gene transcription (Kadmiel & Cidlowski, 2013; Oakley & Cidlowski, 2013). GR depletion in zebrafish resulted in increased body mass and elevated protein and lipid levels, but not carbohydrate levels (Faught & Vijayan, 2019a). The control fish exhibited higher glucose levels

Uncorrected proof

than GR mutant zebrafish, and the stress-induced hyperglycaemia observed in control fish was absent in GR-deficient fish (Faught & Vijayan, 2019a). Zebrafish lacking GR have been reported to be hypercortisolemic (Faught & Vijayan, 2019a). These results were consistent with our observations in GR-deficient fish in this study, confirming that GC signaling correlates with physiological metabolism. Down-regulated hepatic and muscular *cpt1b* expression could be effectively rescued following HC treatment in *star*$^{-/-}$ and *cyp17a2*$^{-/-}$ fish rather than *gr*$^{-/-}$ fish. This further indicates that the promotion of *cpt1b* expression by GC signaling is GR-dependent. Together with the results of relative luciferase activity, it has been demonstrated that GC/Gr signaling positively regulates the transcription of *cpt1b* to maintain nutrient metabolism.

Maintaining a dynamic balance between lipid, carbohydrate and protein metabolism is essential for cellular energy homeostasis (Gale et al., 2004). In mammals, free fatty acids are delivered to the mitochondria, where they undergo fatty acid oxidation to produce adenosine triphosphate (ATP) for survival (Eaton, 2002; Finn & Dice, 2006; Kerner & Hoppel, 2000). In this study, the increased content of non-esterified fatty acids and decreased content of acylcarnitine in fish models with compromised GC/Gr signaling could be attributed to decreased FAO due to aberrant CPT1B regulation in the liver. FAO inhibition has been reported to enhance glucose utilization and promote protein deposition, as *cpt1b* deficiency is associated with increased carbohydrate utilization and protein deposition through remodeling of insulin and protein kinase B (AKT) signaling, which is related to energy homeostasis (Li et al., 2020a). This remodeling of energy homeostasis could partially explain the metabolic phenotype observed in the FAO-inhibited fish models in this study. These findings in fish are also supported by data from mice with impaired mitochondrial fat oxidation, suggesting that this mechanism may be conserved among vertebrates (Morrow et al., 2017; Wicks et al., 2015).

Enhanced body weight gain without increased lipid accumulation was observed in hypocortisolemic *pomca*$^{-/-}$ zebrafish (Shi et al., 2020). However, *star*$^{-/-}$, *cyp17a2*$^{-/-}$, and *gr*$^{-/-}$ fish in this study all exhibited significantly higher lipid content compared to their age-matched control siblings. This unique phenotype, which is distinct among *pomca* mutation models, was abolished when hyperandrogenism was eliminated by additional *cyp17a1* depletion. Using *cyp17a1*$^{-/-}$ and *ar*$^{-/-}$ models, we demonstrated that androgen signaling inhibits *de novo* lipogenesis (DNL) to alleviate lipid deposition (Jia et al., 2024). Mechanistically, in *cyp17a1*$^{-/-}$ fish, chromatin accessibility of DNL genes (*scd* and *fasn*) was significantly increased, and

Uncorrected proof

androgen treatment failed to rescue lipid accumulation in the absence of Ar. The divergent adiposity phenotype between zebrafish and mammalian *pomc* mutants likely stems from species-specific metabolic regulation. While *POMC* deficiency causes early-onset obesity in humans (Krude et al., 1998) and mice (Yaswen et al., 1999), zebrafish *pomca*$^{-/-}$ exhibit increased body weight without adiposity due to concurrent hyperandrogenism. Although transient fat accumulation has been reported at early developmental stages in *pomca*$^{-/-}$ fish (Rajeswari et al., 2024), this may reflect temporal dynamics of metabolic adaptation rather than contradicting the androgen-mediated DNL inhibition. Notably, *pomca*$^{-/-}$ fish maintain relatively higher plasma cortisol and testosterone levels compared to other hypocortisolemic models (*star*$^{-/-}$, *cyp17a2*$^{-/-}$, *gr*$^{-/-}$) (Table 1). This residual androgen production suppresses DNL and prevents obesity, consistent with our previous findings.

Mr exhibits a higher affinity for GC than Gr (Wepler et al., 2020). Rajeswari et al. reported that in *pomca*-deficient zebrafish, the up-regulated *peroxisome proliferator-activated receptor gamma* (*pparγ*), *fasn* and down-regulated *lipoprotein lipase* (*lpl*) were caused by its reduced Gr and enhanced Mr responsiveness (Faught & Vijayan, 2019b). There is accumulating evidence to support that both these receptors are involved in GC-mediated lipid metabolism, among which, Mr activation both mediates postnatal lipid accumulation and cooperatively regulates Gr-mediated lipolysis during stress (Faught & Vijayan, 2019b). Building on this context of differential signaling via Gr and Mr, we sought to identify the specific downstream target of glucocorticoid signaling through which Gr mediates the effects of GC on lipid metabolism. Here, we identify *cpt1b* as a key downstream target of Gr-dependent lipid regulation. This finding is significant given that impaired GC/Gr signaling is a hallmark of obesity, a disease that has reached epidemic proportions worldwide. Hypocortisolism is a group of genetic conditions affecting adrenal gland steroidogenesis and leading to decreased cortisol synthesis (Charmandari et al., 2002). It has been reported that patients with hypocortisolism have an increased BMI and are more prone to obesity (Belkasem A et al., 2021). Despite extensive observational and epidemiological evidence reporting obesity as one of the metabolic syndromes caused by classical hypocortisolism, clinical trial data has failed to demonstrate the mechanism of the metabolic syndrome itself in hypocortisolism and obesity. Our findings demonstrate that cortisol directly regulates *cpt1b* via Gr to promote FAO, with our *gr*$^{-/-}$ zebrafish serving as a key model. The failure of hydrocortisone to rescue *cpt1b* expression and Cpt1 activity in *gr*$^{-/-}$ fish, in

Uncorrected proof

contrast to its efficacy in *star*$^{-/-}$ and *cyp17a2*$^{-/-}$ fish, provides strong evidence that this regulatory axis is primarily Gr-dependent. The compromised GC/Gr signaling models in this study will refine our understanding of the systemic developmental consequences and metabolic features by providing insights into the relationship between hypocortisolism and FAO activity and the significance of plasma adrenal steroid profiles for lipid metabolism.

When extrapolating our findings to human physiology, it is important to consider the differences in steroidogenesis between species. For example, unlike humans, teleosts lack *aldosterone synthase*, and cortisol functions as both a glucocorticoid and a mineralocorticoid by binding to Gr and Mr (Guh et al., 2015). Furthermore, the zebrafish genome harbors paralogs of certain steroidogenic enzymes (e.g., *cyp17a2*) (Shi et al., 2022), reflecting teleost-specific genome duplication and potential subfunctionalization. Despite these differences, the central mechanism elucidated here, glucocorticoid signaling promoting fatty acid oxidation via the transcriptional activation of target genes may be conserved in vertebrates. For instance, glucocorticoids have been demonstrated to regulate FAO by modulating the expression of *PPARα*, which supports the conserved role of glucocorticoid signaling in lipid metabolism regulation (Lemberger et al., 1996). Thus, our findings offer mechanistic insights into the metabolic consequences of impaired glucocorticoid signaling that may be relevant to human conditions such as hypocortisolism and glucocorticoid resistance, though confirmation in mammalian systems is needed in future studies.

Despite these findings, several limitations should be considered. The specific glucocorticoid response element (GRE) motif (GGCAGTGTGTCT) reported in mice (Hagerty et al., 2001) may not be conserved in teleosts. Therefore, its presence and the underlying regulatory mechanism in the zebrafish remain to be determined. This precludes the definitive identification of the direct molecular target through which Gr regulates *cpt1b* in zebrafish. Unfortunately, due to the lack of a suitable antibody against zebrafish Gr, chromatin immunoprecipitation sequencing (ChIP-seq) could not be performed in this study to definitively identify *cpt1b* as its direct transcriptional target. Future studies employing techniques such as ChIP-seq based on available antibody or protein-tag knock-in strategies will be required to further elucidate the molecular mechanisms by which Gr regulates *cpt1b*, including the identification of zebrafish-specific GREs or Gr-interacting transcription factors. On the other hand, we cannot entirely exclude the potential involvement of Mr in the observed metabolic phenotypes, particularly in the *pomca*$^{-/-}$ model, as

Uncorrected proof

the specific contribution of Mr signaling was not experimentally dissected. Future studies utilizing zebrafish *mr* knockout models will be valuable to delineate the distinct and interactive roles of Gr and Mr in lipid homeostasis.

It should also be noted that all *in vivo* analyses in this study were performed exclusively on adult male fish. This approach was chosen to minimize physiological variability arising from sex differences and cyclical hormonal fluctuations in females, thereby enhancing the robustness of our data and allowing us to establish a stable metabolic baseline for investigating glucocorticoid signaling specifically. This male-focused design is consistent with common practice in the field (Li et al., 2020a; Wang et al., 2024; Xi et al., 2023) and is further supported by the well-established role of androgens in lipid metabolism and their strong interaction with the HPI axis. However, we acknowledge that this approach precludes the examination of potential female-specific effects. Therefore, future studies should therefore investigate whether the regulatory mechanisms identified here are conserved in females or modulated by sex-specific hormonal contexts.

uncorrected proof

DATA ACCESSIBILITY

The transcriptomics raw data files in this article are available in Sequence Read Archive (SRA) at NCBI, and the bioproject is PRJNA1436836.

SUPPLEMENTARY DATA

Supplementary data to this article can be found online.

COMPETING INTERESTS

The authors declare that they have no competing interests.

AUTHORS' CONTRIBUTIONS

Y. Z: Resources, investigation, formal analysis, data curation, methodology. S. S: Resources, methodology. X. L: Resources, investigation, formal analysis, methodology. C. S: Resources, methodology. X. W, J. X: Investigation. Q. L, X. J, J. H: Data curation. G. Z: Conceptualization, writing-original draft, project administration, funding acquisition. Z. Y: Writing-review & editing, supervision, project administration, funding acquisition. All authors read and approved the final version of the manuscript.

ACKNOWLEDGEMENTS

We thank Mr. Wenyou Chen, Institute of Hydrobiology, Chinese Academy of Sciences, for taking care of the zebrafish stocks. We also appreciate Mr. Xin Wang, Institute of Hydrobiology, Chinese Academy of Sciences, for his assistance with micro-CT. The schematic diagram of figure 8 was created using BioGDP.com (Agreement number: GDP20269MM4HH) (Jiang et al., 2025). The authors confirm that the illustrations comply with BioGDP's Terms of Use for academic publishing.

FINANCIAL DISCLOSURE STATEMENT

This work was supported by the National Key Research and Development Program, China (2022YFF1000300 to ZY and 2022YFD2401800 to GZ), the Foundation of Hubei Hongshan Laboratory (2021hskf013 to GZ and 2021hszd021 to ZY), the State Key Laboratory of Freshwater Ecology and Biotechnology (2016FBZ05 to ZY), Hubei Provincial Natural Science

Uncorrected proof

649 Foundation (2025AFA063 to GZ), and Science and Technology Research and Development
650 Projects of China National Fisheries Corp (CNFCCA2025001 to ZY).
651

uncorrected proof

REFERENCES

Bacila I, Lawrence NR, Mahdi S, et al. 2022. Health status of children and young persons with congenital adrenal hyperplasia in the UK (CAH-UK): a cross-sectional multi-centre study. *European Journal of Endocrinology*, **187**(4): 543–553.

Bacila I, Oberski L, Li N, et al. 2025. Steroid 21-hydroxylase deficiency dysregulates essential molecular pathways of metabolism and energy provision. *Biology Open*, **14**(9): bio061977

Belkasem A, Abdurahman, Ibtisam H. 2021. Overweight and obesity among children with congenital adrenal hyperplasia (CAH)- an experience at tripoli university hospital, Tripoli, Libya. *Internet Journal of Pediatrics and Neonatology*, **3**(1): 06–09.

Caron KM, Soo SC, Parker KL. 1998. Targeted disruption of StAR provides novel insights into congenital adrenal hyperplasia. *Endocrine Research*, **24**(3-4): 827–834.

Charmandari E, Weise M, Bornstein SR, et al. 2002. Children with classic congenital adrenal hyperplasia have elevated serum leptin concentrations and insulin resistance: potential clinical implications. *Journal of Clinical Endocrinology Metabolism*, **87**(5): 2114–2120.

Dinarello A, Licciardello G, Fontana CM, et al. 2020. Glucocorticoid receptor activities in the zebrafish model: a review. *The Journal of Endocrinology*, **247**(3): R63–R82.

Eachus H, Zaucker A, Oakes JA, et al. 2017. Genetic disruption of 21-hydroxylase in zebrafish causes interrenal hyperplasia. *Endocrinology*, **158**(12): 4165–4173.

Eaton S. 2002. Control of mitochondrial beta-oxidation flux. *Progress in Lipid Research*, **41**(3): 197–239.

Falhammar H, Frisén L, Hirschberg AL, et al. 2015. Increased cardiovascular and metabolic morbidity in patients with 21-hydroxylase deficiency: a swedish population-based national cohort study. *The Journal of Clinical Endocrinology and Metabolism*, **100**(9): 3520–3528.

Faught E, Vijayan MM. 2019a. Loss of the glucocorticoid receptor in zebrafish improves muscle glucose availability and increases growth. *American Journal of Physiology Endocrinology and Metabolism*, **316**(6): E1093–E1104.

Faught E, Vijayan MM. 2019b. Postnatal triglyceride accumulation is regulated by mineralocorticoid receptor activation under basal and stress conditions. *The Journal of Physiology*, **597**(19): 4927–4941.

Faught E, Vijayan MM. 2022. The mineralocorticoid receptor functions as a key glucose regulator in the skeletal muscle of zebrafish. *Endocrinology*, **163**(11).

Finn PF, Dice JF. 2006. Proteolytic and lipolytic responses to starvation. *Nutrition*, **22**(7-8): 830–844.

Folch J, Lees M, Sloane Stanley GH. 1957. A simple method for the isolation and purification of total lipides from animal tissues. *The Journal of Biological Chemistry*, **226**(1): 497–509.

Gale SM, Castracane VD, Mantzoros CS. 2004. Energy homeostasis, obesity and eating disorders: recent advances in endocrinology. *The Journal of Nutrition*, **134**(2): 295–298.

Gonzalez-Nunez V, Gonzalez-Sarmiento R, Rodríguez RE. 2003. Identification of two proopiomelanocortin genes in zebrafish (*Danio rerio*). *Brain Research Molecular Brain Research*, **120**(1): 1–8.

Guh YJ, Lin CH, Hwang PP. 2015. Osmoregulation in zebrafish: ion transport mechanisms and functional regulation. *Experimental and Clinical Sciences*, **14**: 627–659.

Hagerty T, Morgan WW, Elango N, et al. 2001. Identification of a glucocorticoid-responsive element in the promoter region of the mouse tyrosine hydroxylase gene. *Journal of Neurochemistry*, **76**(3): 825–834.

Ishii T, Hasegawa T, Pai CI, et al. 2002. The roles of circulating high-density lipoproteins and trophic hormones in the phenotype of knockout mice lacking the steroidogenic acute regulatory protein. *Molecular Endocrinology*, **16**(10): 2297–2309.

Jia JY, Chen GH, Shu TT, et al. 2024. Androgen signaling inhibits de novo lipogenesis to alleviate lipid deposition in zebrafish. *Zoological Research*, **45**(2): 355–366.

Jiang S, Li H, Zhang L, et al. 2025. Generic Diagramming Platform (GDP): a comprehensive database of high-quality biomedical graphics. *Nucleic Acids Research*, **53**(D1): D1670–D1676.

Kadmiel M, Cidlowski JA. 2013. Glucocorticoid receptor signaling in health and disease. *Trends in Pharmacological Sciences*, **34**(9): 518–530.

Kara L, Cicek D, Siraz UG, et al. 2024. Congenital adrenal hyperplasia with combined 21-hydroxylase deficiency and 17α-hydroxylase/17,20-lyase deficiency: An undervirilized male. *European Journal of Medical Genetics*, **69**:

Uncorrected Proof

104952.
Kerner J, Hoppel C. 2000. Fatty acid import into mitochondria. *Biochim Biophys Acta*, **1486**(1): 1–17.
Kim MS, Ryabets-Lienhard A, Dao-Tran A, et al. 2015. Increased abdominal adiposity in adolescents and young adults with classical congenital adrenal hyperplasia due to 21-hydroxylase deficiency. *The Journal of Clinical Endocrinology and Metabolism*, **100**(8): E1153–E1159.
Krude H, Biebermann H, Luck W, et al. 1998. Severe early-onset obesity, adrenal insufficiency and red hair pigmentation caused by POMC mutations in humans. *Nature genetics*, **19**(2): 155–157.
Lau ES, Zhang Z, Qin M, et al. 2016. Knockout of zebrafish ovarian aromatase gene (*cyp19a1a*) by TALEN and CRISPR/Cas9 leads to all-male offspring due to failed ovarian differentiation. *Scientific Reports*, **6**: 37357.
Lemberger T, Saladin R, Vázquez M, et al. 1996. Expression of the peroxisome proliferator-activated receptor alpha gene is stimulated by stress and follows a diurnal rhythm. *Journal of Biological Chemistry*, **271**(3): 1764–1769.
Li LY, Li JM, Ning LJ, et al. 2020a. Mitochondrial fatty acid beta-oxidation inhibition promotes glucose utilization and protein deposition through energy homeostasis remodeling in fish. *The Journal of Nutrition*, **150**(9): 2322–2335.
Li N, Oakes JA, Storbeck KH, et al. 2020b. The P450 side-chain cleavage enzyme Cyp11a2 facilitates steroidogenesis in zebrafish. *The Journal of Endocrinology*, **244**(2): 309–321.
Lin JC, Hu S, Ho PH, et al. 2015. Two zebrafish *hsd3b* genes are distinct in function, expression, and evolution. *Endocrinology*, **156**(8): 2854–2862.
Livak KJ, Schmittgen TD. 2001. Analysis of relative gene expression data using real-time quantitative PCR and the 2(-Delta Delta C(T)) method. *Methods*, **25**(4): 402–408.
Lopes V, Filho AB, Yoshinaga M, et al. 2022. Carnitine palmitoyl transferase I: conformational changes induced by long-chain fatty acyl CoA ligands. *Journal of Molecular Graphics and Modelling*, **112**: 108125.
Morrow RM, Picard M, Derbeneva O, et al. 2017. Mitochondrial energy deficiency leads to hyperproliferation of skeletal muscle mitochondria and enhanced insulin sensitivity. *Proceedings of the National Academy of Sciences of the United States of America*, **114**(10): 2705–2710.
Nipu N, Antomagesh F, Faught E, et al. 2022. Glucocorticoid receptor activation reduces food intake independent of hyperglycemia in zebrafish. *Scientific Reports*, **12**(1): 15677.
Oakley RH, Cidlowski JA. 2013. The biology of the glucocorticoid receptor: new signaling mechanisms in health and disease. *The Journal of Allergy and Clinical Immunology*, **132**(5): 1033–1044.
Parajes S, Griffin A, Taylor AE, et al. 2013. Redefining the initiation and maintenance of zebrafish interrenal steroidogenesis by characterizing the key enzyme cyp11a2. *Endocrinology*, **154**(8): 2702–2711.
Peng XY, Shang GH, Wang WQ, et al. 2017. Fatty acid oxidation in zebrafish adipose tissue is promoted by 1α,25(OH)2D3. *Cell Reports*, **19**(7): 1444–1455.
Raffan E, Dennis RJ, O'donovan CJ, et al. 2016. A deletion in the canine *POMC* gene is associated with weight and appetite in obesity-prone labrador retriever dogs. *Cell Metabolism*, **23**(5): 893–900.
Rajeswari JJ, Faught E, Santos H, et al. 2024. Mineralocorticoid receptor activates postnatal adiposity in zebrafish lacking proopiomelanocortin. *Journal of Cellular Physiology*, **239**(12): e31428.
Ruan Y, Li X, Wang X, et al. 2024. New insights into the all-testis differentiation in zebrafish with compromised endogenous androgen and estrogen synthesis. *PLoS Genetics*, **20**(3): e1011170.
Sahakitrungruang T, Soccio RE, Lang-Muritano M, et al. 2010. Clinical, genetic, and functional characterization of four patients carrying partial loss-of-function mutations in the steroidogenic acute regulatory protein (StAR). *The Journal of Clinical Endocrinology and Metabolism*, **95**(7): 3352–3359.
Schubert T, Reisch N, Naumann R, et al. 2022. *CYP21A2* gene expression in a humanized 21-hydroxylase mouse model does not affect adrenocortical morphology and function. *Journal of the Endocrine Society*, **6**(6): bvac062.
Shang GH, Peng XY, Ji C, et al. 2019. Steroidogenic acute regulatory protein and luteinizing hormone are required for normal ovarian steroidogenesis and oocyte maturation in zebrafishdagger. *Biology of Reproduction*, **101**(4): 760–770.
Shi C, Lu Y, Zhai G, et al. 2020. Hyperandrogenism in POMCa-deficient zebrafish enhances somatic growth without increasing adiposity. *Journal of Molecular Cell Biology*, **12**(4): 291–304.
Shi C, Zhang YQ, Lu Y, et al. 2025. Insights into the role of Fsh signaling in ovarian differentiation of chorionic gonadotropin α (*cgα*)-deficient zebrafish. *Zoological Research*, **46**(3): 695–708.
Shi SC, Shu TT, Li X, et al. 2022. Characterization of the interrenal gland and sexual traits development in

Uncorrected proof

cyp17a2-deficient zebrafish. *Frontiers in Endocrinology* **13**: 910639.

Söder J, Höglund K, Dicksved J, et al. 2019. Plasma metabolomics reveals lower carnitine concentrations in overweight Labrador Retriever dogs. *Acta Veterinaria Scandinavica*, **61**(1): 10.

Thisse C, Thisse B. 2008. High-resolution in situ hybridization to whole-mount zebrafish embryos. *Nature Protocols*, **3**(1): 59–69.

Van Der Valk ES, Kleinendorst L, Delhanty PJD, et al. 2022. Obesity and hyperphagia with increased defective ACTH: a novel POMC variant. *The Journal of Clinical Endocrinology and Metabolism*, **107**(9): E3699–E3704.

Vitellius G, Trabado S, Bouligand J, et al. 2018. Pathophysiology of glucocorticoid signaling. *Annales D Endocrinologie*, **79**(3): 98–106.

Wang JX, Zhang YY, Qian YC, et al. 2024. Inhibition of mitochondrial citrate shuttle alleviates metabolic syndromes induced by high-fat diet. *American Journal of Physiology-cell Physiology*, **327**(3): C737–C749.

Wepler M, Preuss JM, Merz T, et al. 2020. Impact of downstream effects of glucocorticoid receptor dysfunction on organ function in critical illness-associated systemic inflammation. *Intensive Care Medicine Experimental*, **8**(Suppl 1): 37.

Westerfield M. 2020. The zebrafish book, a guide for the laboratory use of zebrafish (*Danio rerio*). OR 4rd ed. Eugene: the University of Oregon Press.

Wicks SE, Vandanmagsar B, Haynie KR, et al. 2015. Impaired mitochondrial fat oxidation induces adaptive remodeling of muscle metabolism. *Proceedings of the National Academy of Sciences of the United States of America*, **112**(25): E3300–E3309.

Xi LW, Zhai G, Liu YL, et al. 2023. Attenuated glucose uptake promotes catabolic metabolism through activated AMPK signaling and impaired insulin signaling in zebrafish. *Frontiers in Nutrition*, **10**: 1187283.

Yaswen L, Diehl N, Brennan MB, et al. 1999. Obesity in the mouse model of pro-opiomelanocortin deficiency responds to peripheral melanocortin. *Nature medicine*, **5**(9): 1066–1070.

Yin Y, Tang H, Liu Y, et al. 2017. Targeted disruption of aromatase reveals dual functions of *cyp19a1a* during sex differentiation in zebrafish. *Endocrinology*, **158**(9): 3030–3041.

Zemel MB, Shi H. 2000. Pro-opiomelanocortin (POMC) deficiency and peripheral melanocortins in obesity. *Nutrition Reviews*, **58**(6): 177–180.

Zhai G, Shu TT, Xia YG, et al. 2018. Characterization of sexual trait development in *cyp17a1*-deficient zebrafish. *Endocrinology*, **159**(10): 3549–3562.

Zhai G, Shu TT, Yu GQ, et al. 2022. Augmentation of progestin signaling rescues testis organization and spermatogenesis in zebrafish with the depletion of androgen signaling. *eLife*, **11**: e66118.

Zhang L, Wan M, Tohti R, et al. 2022. Requirement of zebrafish *adcy3a* and *adcy5* in melanosome dispersion and melanocyte stripe formation. *International Journal of Molecular Sciences*, **23**(22): 14182.

Zhang Q, Ye D, Wang H, et al. 2020. Zebrafish *cyp11c1* knockout reveals the roles of 11-ketotestosterone and cortisol in sexual development and reproduction. *Endocrinology*, **161**(6): bqaa048.

uncorrected proof

FIGURE LEGENDS

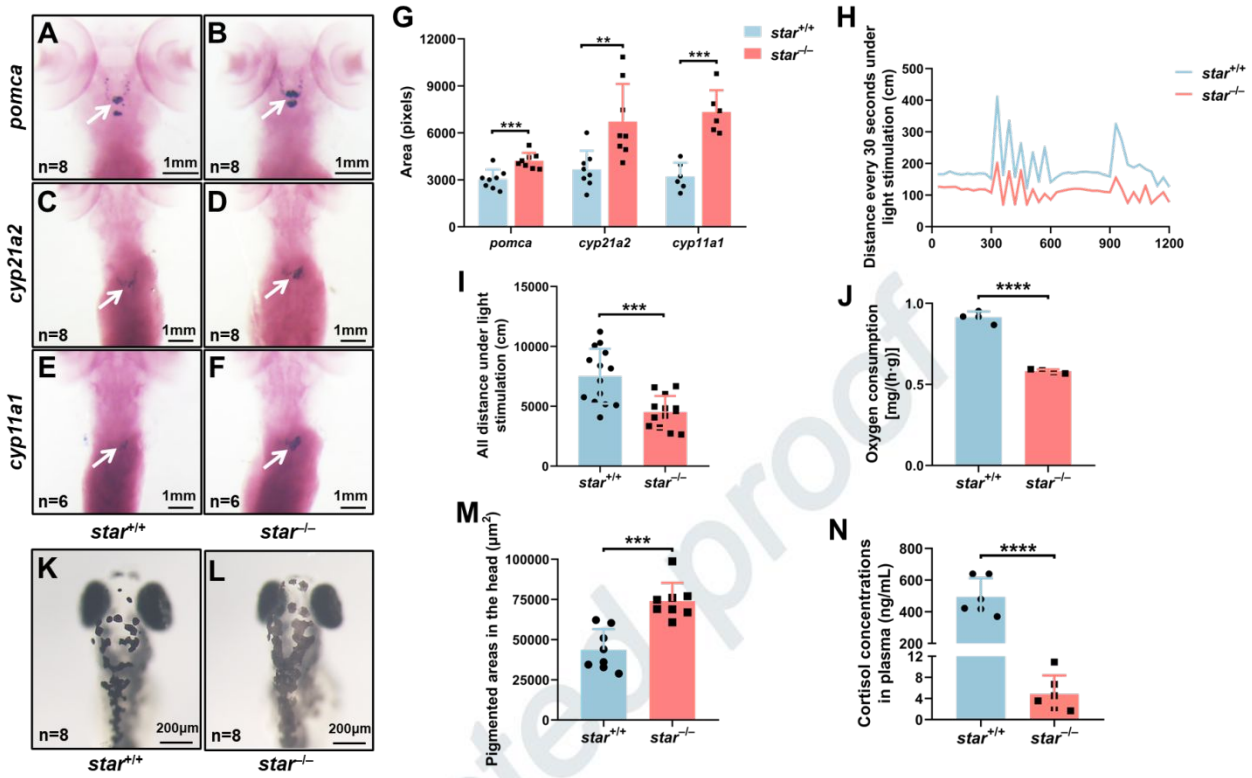

Figure 1. *star*-depletion resulted in inactivated pituitary-interrenal axis

A–F: WISH analyses probes of *pomca* (A, B, *n*=8), *cyp21a2* (C, D, *n*=8), *cyp11a1* (E, F, *n*=6) in control and *star*-deficient fish at 5 dpf. G: Quantitative and statistical analysis results of WISH. H: Control (*n*=14) and *star*-deficient fish (*n*=13) analyzed for the movement distance every 30 seconds within 20 min under the alternating 5 min intervals of light and dark. I: All distances traveled by light stimulation in 20 min. J: The oxygen consumption of control and *star*-deficient fish after 2 days of starvation (*n*=4/group). K, L: Images of control and *star*-deficient fish at 4 dpf exposed to illumination for 30 min (*n*=8). M: The area of melanin in the region of interest quantitative and statistical analysis results. N: The cortisol concentrations of control and *star*-deficient fish (*n*=6). **: $P<0.01$; ***: $P<0.001$; ****: $P<0.0001$.

Uncorrected Proof

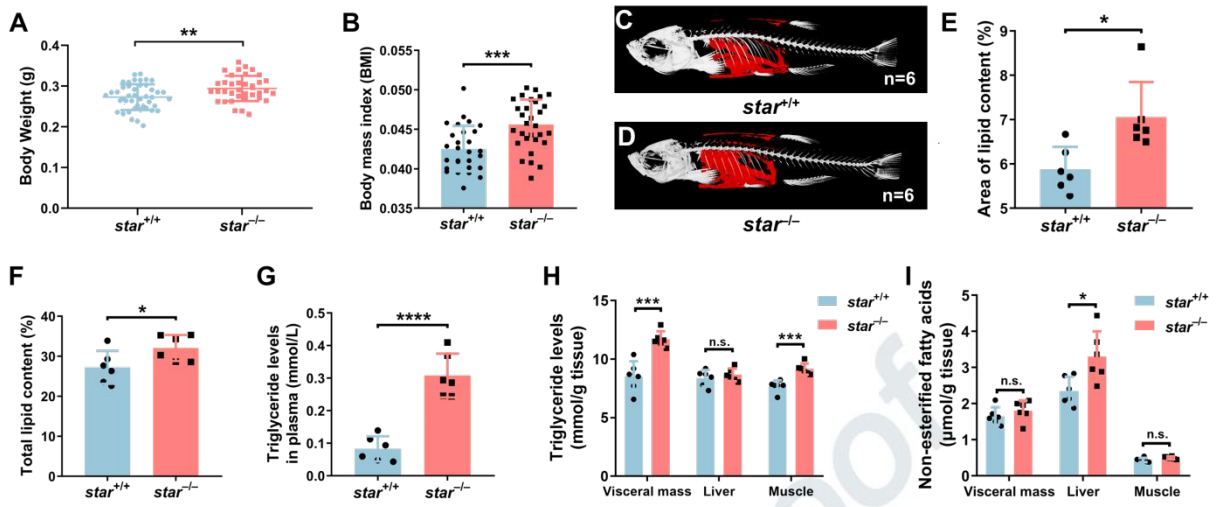

Figure 2. *star*-depletion resulted in lipid accumulation and decreased FAO

A: Body weight of control (n=44) and *star*-deficient fish (n=37). B: Body mass index of control (n=28) and *star*-deficient fish (n=30) at 4 mpf. C, D: The micro-CT images of control and *star*-deficient fish (n=6), the bone is shown in white, and the lipid is shown in red. E: The area of lipid as a percentage of total area in the micro-CT images of control and *star*-deficient fish. F: Total lipid content of control and *star*-deficient fish (n=6). G: Triglyceride levels in plasma of control and *star*-deficient fish (n=6). H: Triglyceride levels in various tissues of control and *star*-deficient fish (n=6). I: Non-esterified fatty acids levels in various tissues of control and *star*-deficient fish (n=6). n.s.: Not significant; *: P<0.05; **: P<0.01; ***: P<0.001; ****: P<0.0001.

uncorrected proof

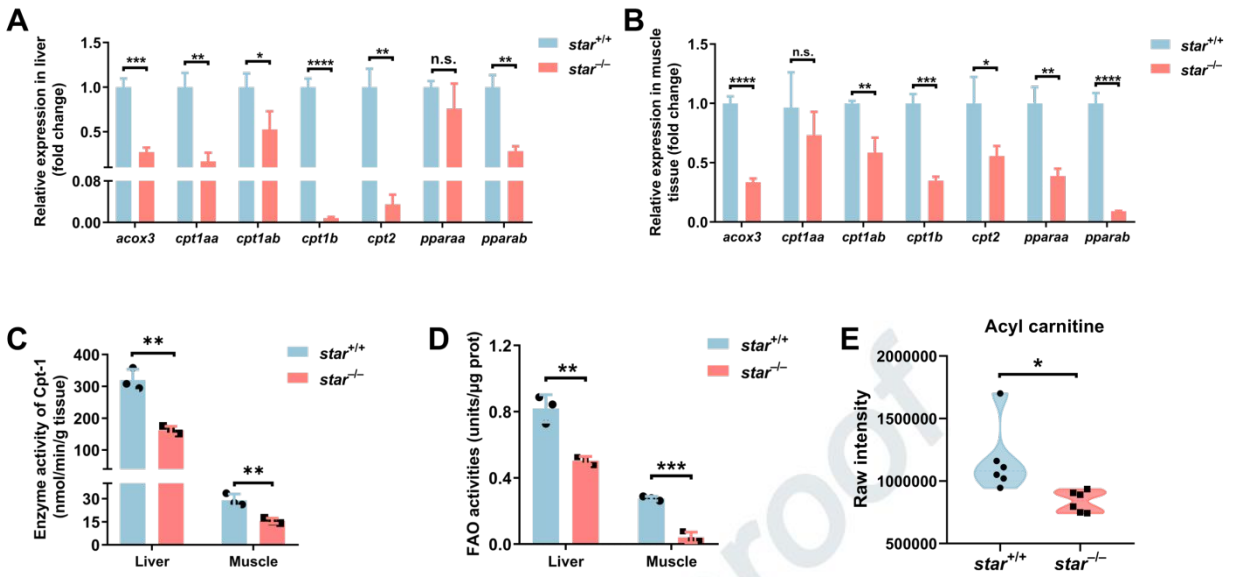

Figure 3. *star*-depletion resulted in decreased FAO

A: The expression analysis of *acox3*, *cpt1aa*, *cpt1ab*, *cpt1b*, *cpt2*, *pparaa*, and *pparab* in liver of control and *star*-deficient fish (n=3). B: The expression analysis of *acox3*, *cpt1aa*, *cpt1ab*, *cpt1b*, *cpt2*, *pparaa*, and *pparab* in muscle of control and *star*-deficient fish (n=3). C: The enzyme activity of Cpt-1 in liver and muscle of control and *star*-deficient fish (n=3). D: The FAO activities in liver and muscle of control and *star*-deficient fish (n=3). E: The acly carnitine content of control and *star*-deficient fish (n=6) as measured using metabolomic analysis. n.s.: Not significant; *: P<0.05; **: P<0.01; ***: P<0.001; ****: P<0.0001.

uncorrected proof

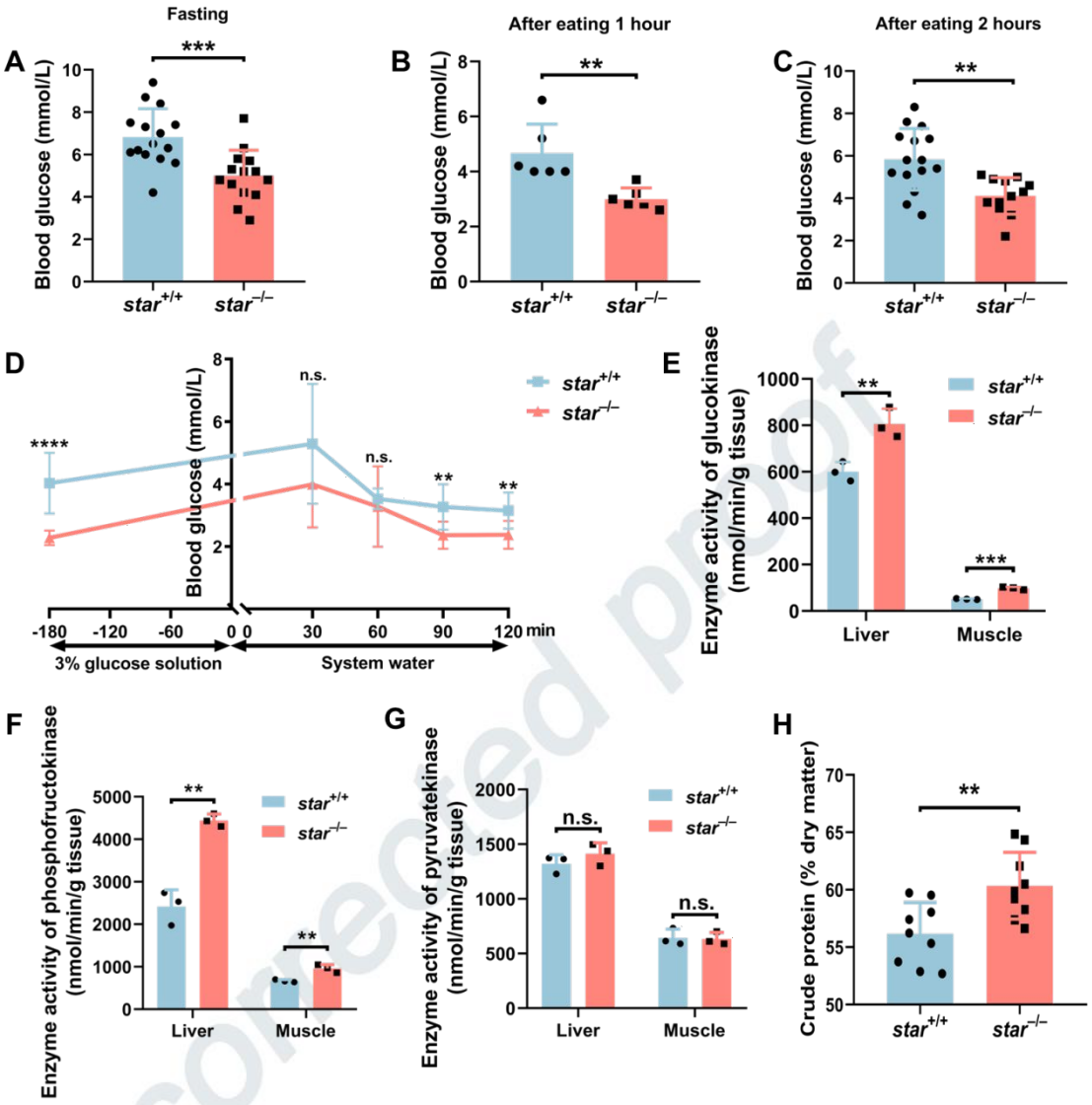

Figure 4. *star*-depletion resulted in increased glycolysis and protein deposition

A: Blood glucose at 0 hours after feeding in control (n=15) and *star*-deficient fish (n=14) fish. B: Blood glucose at 1 hour after feeding in control (n=6) and *star*-deficient fish (n=6) fish. C: Blood glucose at 2 hours after feeding in control (n=15) and *star*-deficient fish (n=12) fish. D: Blood glucose in control (n=7) and *star*-deficient fish (n=10) fish after the glucose tolerance test for 30-, 60-, 90-, and 120-minutes. E-G: The enzyme activity of glucokinase (E), phosphofructokinase (F), pyruvatekinase (G) in liver and muscle of control and *star*-deficient fish (n=3). H: The crude protein of control and *star*-deficient fish (n=9). n.s.: Not significant; **: P<0.01; ***: P<0.001; ****: P<0.0001.

Uncorrected proof

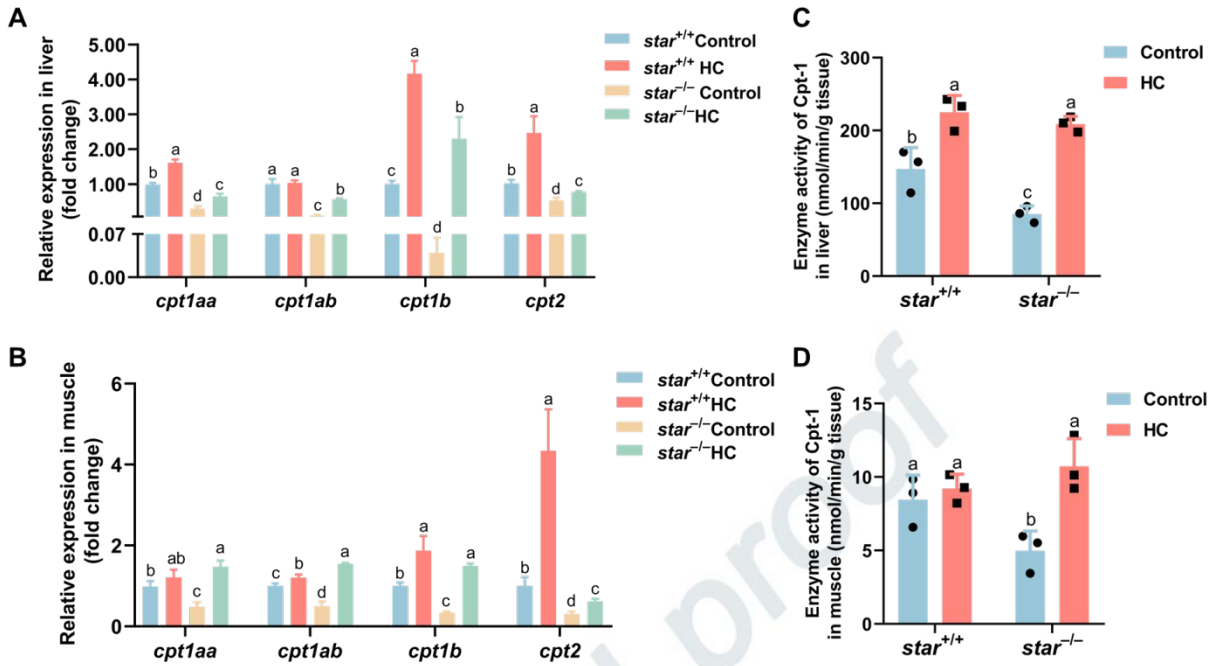

Figure 5. Hydrocortisone treatment rescued the expression of *cpt1*, *cpt2* and the enzyme activity of Cpt1 in *star*-deficient zebrafish

A, B: The expression analysis of *cpt1aa*, *cpt1ab*, *cpt1b*, and *cpt2* in liver (A) and muscle (B) of control fish and control fish administered with hydrocortisone (5 mg/L), *star*-deficient fish and *star*-deficient fish administered with hydrocortisone (5 mg/L) for 24 hours (*n*=3). C, D: The enzyme activity of Cpt-1 in liver (C) and muscle (D) of control fish and control fish administered with hydrocortisone (5 mg/L), *star*-deficient fish and *star*-deficient fish administered with hydrocortisone (5 mg/L) for 10 days (*n*=3). Different letters in the bar chart represent levels with significant differences.

uncorrected proof

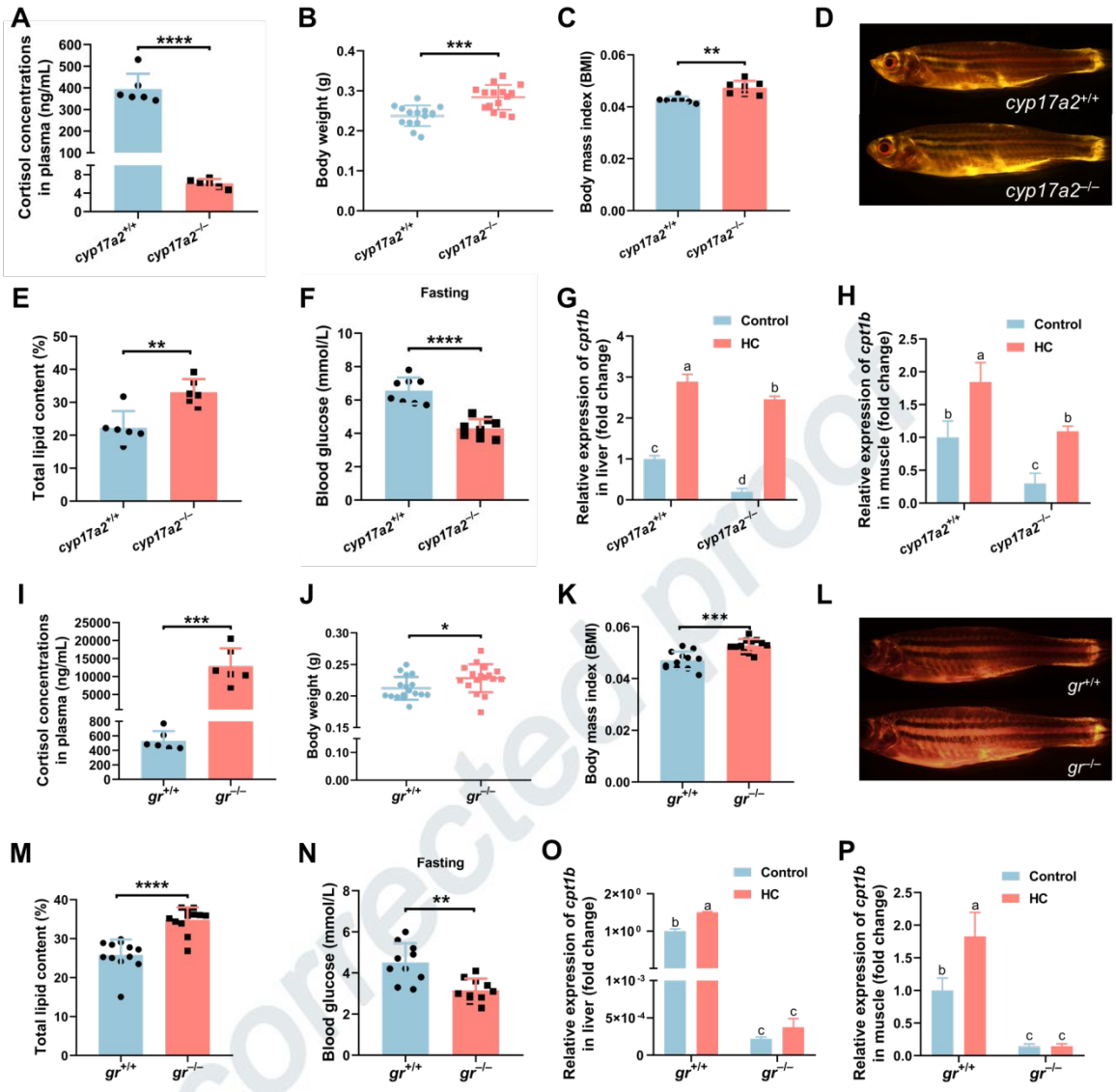

Figure 6. *cyp17a2*- and *gr*-depletion resulted in decreased expression of *cpt1b* and lipid accumulation

A, I: The cortisol concentration of *cyp17a2*- (A, *n*=6) and *gr*-deficient fish (I, *n*=6) compared to their control siblings. B, J: Body weight of *cyp17a2*- (B, *n*=15) and *gr*-deficient fish (J, *n*=17) compared to their control siblings. C, K: Body mass index of *cyp17a2*- (C, *n*=7) and *gr*-deficient fish (K, *n*=12) compared to their control siblings. D, L: Nile red staining of *cyp17a2*- (D, n=3) and *gr*-deficient fish (L, n=3) compared to their control siblings. E, M: Total lipid content of *cyp17a2*- (E, *n*=6) and *gr*-deficient fish (M, *n*=12) compared to their control siblings. F, N: Blood glucose at fasting of *cyp17a2*- (F, *n*=8) and *gr*-deficient fish (N, *n*=10) compared to their control siblings. G, H: The expression of *cpt1b* in liver and muscle of control fish and control

Uncorrected proof

fish administered with hydrocortisone (5 mg/L), *cyp17a2*-deficient fish, *cyp17a2*-deficient fish administered with hydrocortisone (5 mg/L) for 24 hours (n=3). O, P: The expression analysis of *cpt1b* in liver and muscle of control fish, control fish administered with hydrocortisone (5 mg/L), *gr*-deficient fish, *gr*-deficient fish administered with hydrocortisone (5 mg/L) for 24 hours (n=3). *: P<0.05; **: P<0.01; ***: P<0.001; ****: P<0.0001. Different letters in the bar chart represent levels with significant differences.

uncorrected proof

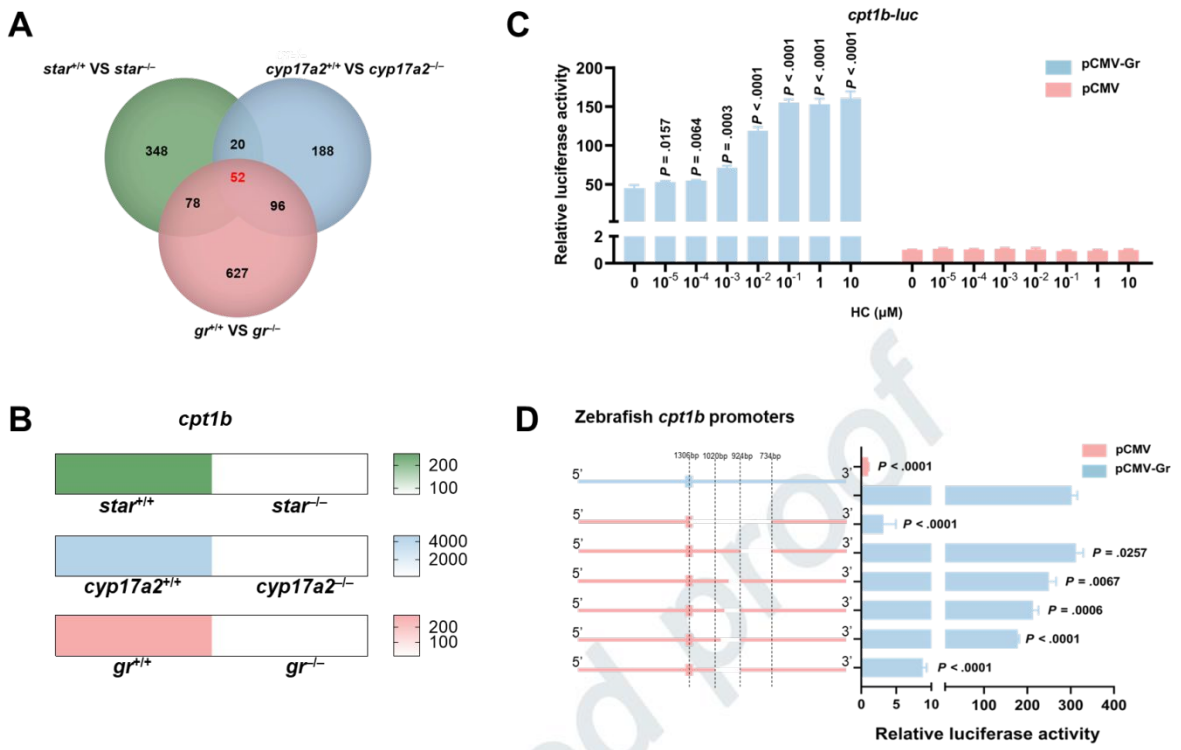

Figure 7. Hydrocortisone enhances the promoter activity of *cpt1b* via glucocorticoid receptor

A: Venn diagram of gene expression profiles in liver of *star*-, *cyp17a2*- and *gr*-deficient fish compared to their control siblings. B: The heatmap of *cpt1b* in liver of *star*-, *cyp17a2*- and *gr*-deficient fish compared to their control siblings. C: The firefly luciferase reporter vector containing zebrafish *cpt1b* promoter (*cpt1b*-luc) were transfected into HEK 293T cells together with the pRT-TK vector containing the Renilla luciferase reporter, the Gr expression vector (pCMV-Gr) or the empty control expression vector (PCMV) and treated with hydrocortisone (10 pM-10 μM). In the presence of pCMV-Gr, hydrocortisone significantly increased the promoter activity of *cpt1b* in a dose-dependent manner. D: A series deletion on *cpt1b*-luc was transfected into HEK 293T cells treated with 0.1 μM HC. The major binding region of Gr to zebrafish *cpt1b* promoter is ACTTGAGCTG–ATAGTTGT (924–1020bp). *P* values were calculated by one-tailed, one-way analysis of variance followed by Dunnett test against respective controls (vehicle controls, zero dose).

Uncorrected Proof

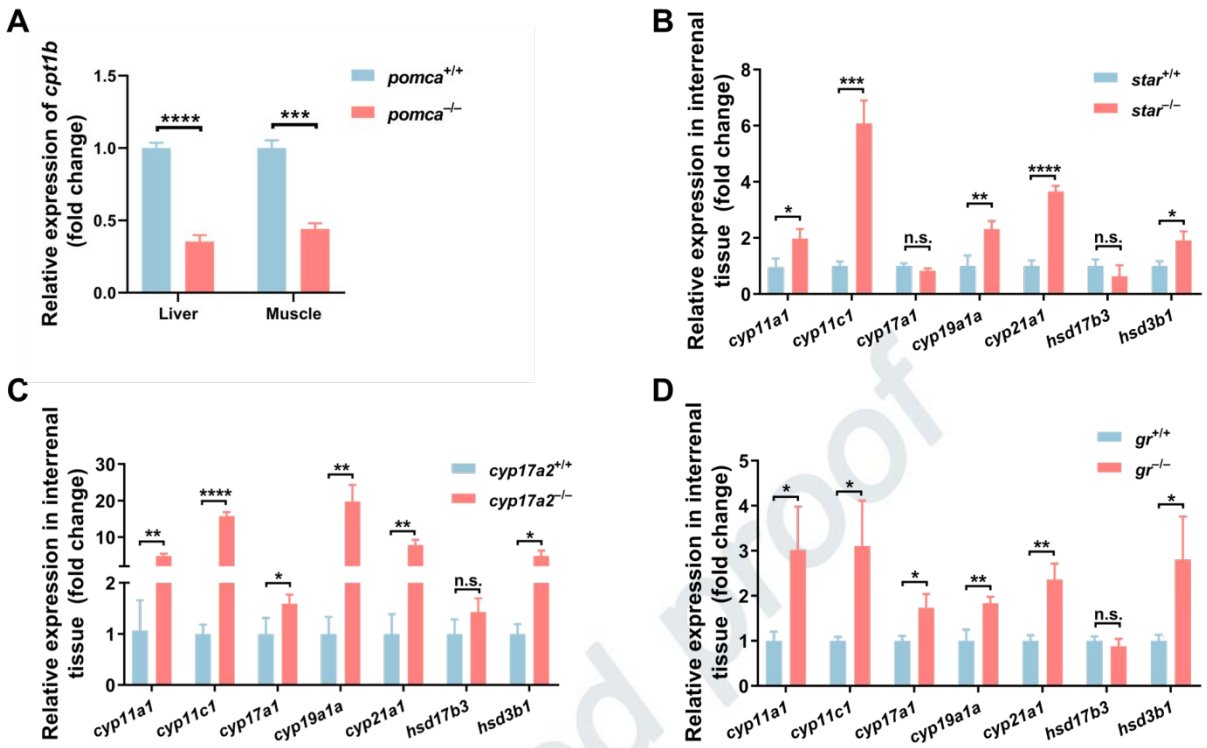

881

882 **Figure 8. The down-regulated *cpt1b* expression in *pomca*-deficient zebrafish and**
883 **comparable *hsd17b3* but up-regulated *hsd3b1* in *star*-, *cyp17a2*- and *gr*-deficient zebrafish**
884 A: The expression of *cpt1b* was decreased in liver and muscle of *pomca*-deficient fish compared
885 to control fish (n=3). B–D: The expression analysis of *cyp11a1*, *cyp11c1*, *cyp17a1*, *cyp19a1a*,
886 *cyp21a1*, *hsd17b3* and *hsd3b1* in interrenal tissue of *star*- (B), *cyp17a2*- (C), *gr*- (D) deficient
887 fish and their control siblings (n=3). n.s.: Not significant; *: P<0.05; **: P<0.01; ***: P<0.001;
888 ****: P<0.0001.

uncorrected Proof

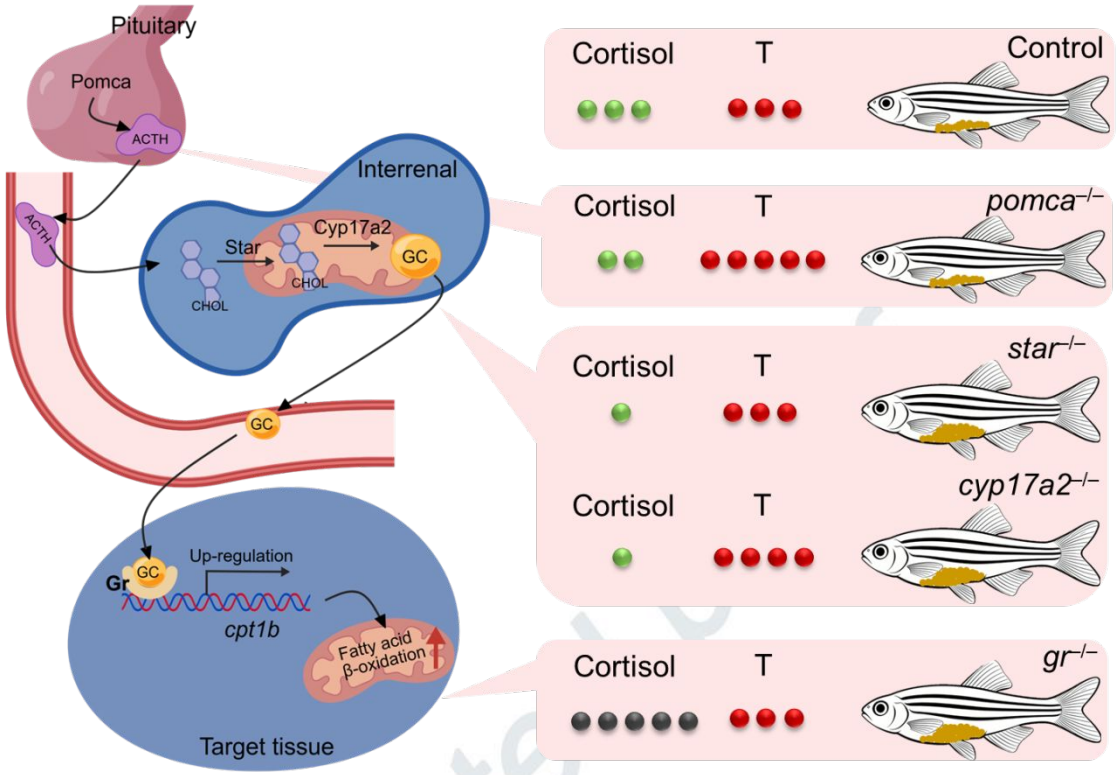

Figure 9. Glucocorticoid (GC) signaling regulates lipid catabolism via Gr-mediated activation of *cpt1b* in zebrafish

Left: The hypothalamic-pituitary-interrenal (HPI) axis governing GC synthesis and the molecular pathway by which GC upregulates *cpt1b* expression and enhances fatty acid β-oxidation (FAO) through Gr. Created with BioGDP.com (Jiang et al., 2025). Right: Plasma cortisol (green dots and gray dots), non-functional cortisol (grey dots), testosterone (red dots) levels and lipid deposition phenotypes (yellow shading) in wild-type control and *pomca*-, *star*-, *cyp17a2*-, *gr*-deficient zebrafish, showing that fat phenotypes resulting from impaired GC signaling are associated with plasma hormone profiles. CHOL: Cholesterol, T: Testosterone, ACTH: Adrenocorticotropic hormone.

Uncorrected Proof

Table 1. The measurement of plasma concentration of cortisol and testosterone, and hepatic *cpt1b* expression in fish at 4 mpf

Gene	Genotype	Cortisol in plasma (pg/μL)		Testosterone in plasma (pg/mL)		*cpt1b* expression in liver (fold change)	
		Content	–/– / +/+	Content	–/– / +/+	Expression	–/– / +/+
star	+/+	494.5±117.3	0.0098	3.679±0.8153	1.248	1.000±0.09592	0.0085
	–/–	4.856±3.507****		4.591±0.7365n.s.		0.0085±0.002353****	
cyp17a2	+/+	394.5±70.60	0.0154	3.449±1.48	2.260	1.000±0.08246	0.1984
	–/–	6.095±0.9346****		7.795±0.6873****		0.1984±0.08402***	
gr	+/+	533.0±133.3	24.1444	3.357±0.778	1.122	1.000±0.05669	0.00022
	–/–	12869±4965***		3.767±0.7194n.s.		0.00022±0.00002****	
pomca	+/+	514.4±149.4	0.0692	2.568±1.158	4.174	1.000±0.037	0.3549
	–/–	35.60±5.867****		10.720±1.189****		0.3549±0.0435****	

n.s.: Not significant; ***: $P<0.001$; ****: $P<0.0001$.

Uncorrected proof

SUPPLEMENTARY FIGURE

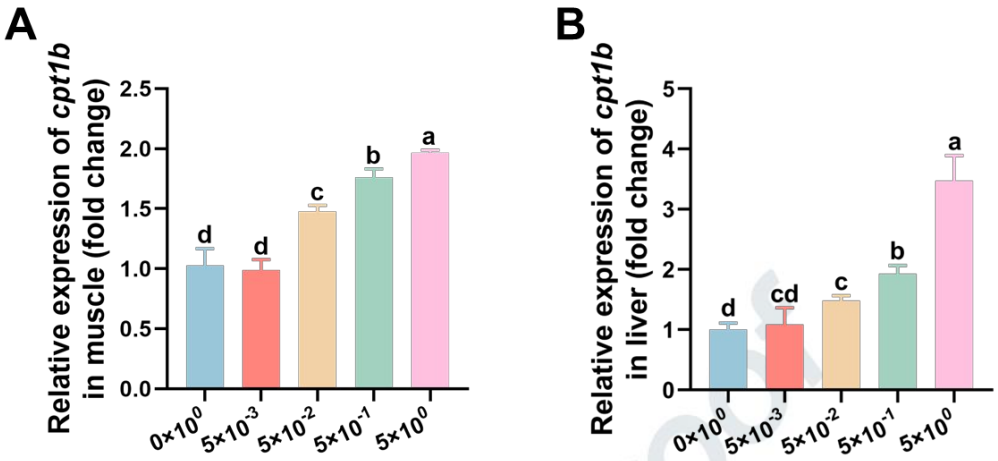

Supplementary Figure S1. HC administration in WT male fish elevated the expression of *cpt1b* both in liver and muscle in a dose-dependent manner

A: The expression analysis of *cpt1b* in liver of WT fish administered with HC at 0.005, 0.05, 0.5 and 5 mg/L. B: The expression analysis of *cpt1b* in muscle of WT fish administered with HC. Different letters in the bar chart represent levels with significant difference.

uncorrected proof

Supplementary Table S1. Primers used in this study

Gene	Primers (5' –3')	Product size (bp)
Genotype examination		
star[a]	F: TGACAGGTAAGAGCACTTTC	407
	R: AGCCTGCATAAAGGAGTCTG	
cyp17a2[a]	F: CTGATGGTGTTTTTCTCTGGG	468
	R: CATCCCTTGCTGTAGCTCTG	
gr[a]	F: GGCAAAAAGCGAGATGAGCG	564
	R: GTCTGATGGCGATCCATCCAG	
qPCR		
β-actin[a]	F: ACTCAGGATGCGGAAACTGG	119
	R: AGGGCAAAGTGGTAAACGCT	
acox3[a]	F: TGGAAGGACATGATGCGCTTT	102
	R: AGGCTGCCGGGCAAAAA	
cpt1aa[a]	F: CATCCTTAGGCCTGCTCTTCAAA	94
	R: ACCATGACACCCCCAACTAACAT	
cpt1ab[a]	F: GACTTCCAATTACGTCAGCGA	189
	R: TGTGCTCTGTCCAGTTTTCTCC	
cpt1b[a]	F: CCTCCATGGGCACGATTGATAA	97
	R: GCAAACAGGATGGCACTCAACA	
cpt2[a]	F: GGTGAACGCCTATCCTCTGG	289
	R: CAACCCTGTCCAGGTGTCTC	
pparaa[a]	F: TGCTGGACTACCAGAACTGTGACA	102
	R: TGCTGGCTGAGAACACTTCTGAG	
pparab[a]	F: TCAGGATACCACTATGGCGTTCAT	100
	R: AGCGGCGTTCACACTTATCGTA	
ORF and promoter amplification		
gr-ORF-F	ATGGATCAAGGAGGACTGGAGAATG	
gr-ORF-R	TCATTTCTGGTGAAAGAGCAGCGGT	
cpt1b-promoter-F	GACTTTGATACTCTTCAAGC	2041
cpt1b-promoter-R	TACAGGCTTAAAGCACAGC	2041

[a]*star, steroidogenic acute regulatory protein. cyp17a2, cytochrome P450, family 17, subfamily A,*

Uncorrected Proof

polypeptide 2. gr, glucocorticoid receptor. β-actin, beta-actin. acox3, acyl-CoA oxidase 3, pristanoyl. cpt1aa, carnitine palmitoyltransferase 1Aa. cpt1ab, carnitine palmitoyltransferase 1Ab. cpt1b, carnitine palmitoyltransferase 1B. cpt2, carnitine palmitoyltransferase 2. gr, glucocorticoid receptor. pparaa, peroxisome proliferator-activated receptor alpha a. pparab, peroxisome proliferator-activated receptor alpha b.

uncorrected proof

Supplementary Table S2. Total lipid content with similar body weight in *star*$^{+/+}$ and *star*$^{-/-}$ fish

Sample	Group	Body Weight	Dry Weight	Lipid	Lipid/Dry Weight	Difference
Con1	*star*$^{+/+}$	**0.334**	0.0917	0.0135	**14.72192**	
Con2	*star*$^{+/+}$	**0.328**	0.0886	0.0134	**15.12415**	
Con3	*star*$^{+/+}$	**0.3181**	0.0893	0.0124	**13.88578**	
Con4	*star*$^{+/+}$	**0.3161**	0.0898	0.0139	**15.47884**	
Con5	*star*$^{+/+}$	**0.301**	0.0814	0.0088	**10.81081**	
Con6	*star*$^{+/+}$	**0.2893**	0.0798	0.0102	**12.78195**	
Con7	*star*$^{+/+}$	0.2871	0.0781	0.0079	10.11524	
Con8	*star*$^{+/+}$	0.2765	0.0792	0.0112	14.14141	
Con9	*star*$^{+/+}$	0.236	0.0572	0.0103	18.00699	*
KO1	*star*$^{-/-}$	0.3752	0.1117	0.0262	23.45568	
KO2	*star*$^{-/-}$	0.3595	0.1008	0.0193	19.14683	
KO3	*star*$^{-/-}$	**0.3568**	0.1079	0.0282	**26.13531**	
KO4	*star*$^{-/-}$	**0.3547**	0.103	0.0222	**21.55340**	
KO5	*star*$^{-/-}$	**0.3374**	0.0957	0.0176	**18.39080**	
KO6	*star*$^{-/-}$	**0.334**	0.1023	0.0226	**22.09189**	
KO7	*star*$^{-/-}$	**0.3114**	0.0888	0.0161	**18.13063**	
KO8	*star*$^{-/-}$	**0.2985**	0.0774	0.0107	**13.82429**	
KO9	*star*$^{-/-}$	**0.2646**	0.0729	0.0103	**14.12894**	

Note:

1. Sample (bolded) represents body weight that is not significantly different in *star*$^{+/+}$ and *star*$^{-/-}$ fish. Their average body weight was 0.3144±0.01670 g and 0.3168±0.03239 g, and the statistical test *P*-value was 0.8776, which represents that body weight was not significantly different from each other. The average whole-body lipid content in *star*$^{+/+}$ and *star*$^{-/-}$ fish was 13.80±1.755% and 18.02%±3.520%, respectively, and the statistical test *P*-value was 0.0253 (*).

2. *: represents the significance of the difference in whole-body lipid content of *star*$^{+/+}$ fish and body weight-matched *star*$^{-/-}$ fish.

Uncorrected proof

Supplementary Table S3. Crude protein content with similar body weight in *star*$^{+/+}$ and *star*$^{-/-}$ fish

Sample	Group	Body Weight	Dry Weight	Crude Protein	Crude Protein/Dry Weight	Difference
Con1	*star*$^{+/+}$	**0.2735**	0.0765	0.043015415	**56.2293**	
Con2	*star*$^{+/+}$	**0.2608**	0.0748	0.0382535	**55.3307**	
Con3	*star*$^{+/+}$	**0.2463**	0.0665	0.03145599	**59.7173**	
Con4	*star*$^{+/+}$	**0.243**	0.0659	0.034710807	**58.0478**	
Con5	*star*$^{+/+}$	**0.2321**	0.0662	0.039712005	**52.8691**	
Con6	*star*$^{+/+}$	**0.2279**	0.0646	0.034999344	**53.7319**	
Con7	*star*$^{+/+}$	0.2258	0.0591	0.041387364	59.5223	
Con8	*star*$^{+/+}$	0.2161	0.0594	0.035177679	57.4067	
Con9	*star*$^{+/+}$	0.2094	0.0597	0.03409958	52.6901	*
KO1	*star*$^{-/-}$	0.2993	0.0821	0.040586368	57.3691	
KO2	*star*$^{-/-}$	0.299	0.0769	0.03822617	62.0597	
KO3	*star*$^{-/-}$	0.2789	0.0706	0.040037693	64.8415	
KO4	*star*$^{-/-}$	**0.2756**	0.0711	0.047723909	**60.4979**	
KO5	*star*$^{-/-}$	**0.2751**	0.0707	0.038552676	**56.6304**	
KO6	*star*$^{-/-}$	**0.2682**	0.0664	0.042721826	**64.3401**	
KO7	*star*$^{-/-}$	**0.2648**	0.0678	0.043014007	**59.8619**	
KO8	*star*$^{-/-}$	**0.2519**	0.0656	0.047100031	**58.2716**	
KO9	*star*$^{-/-}$	**0.2486**	0.0651	0.045778099	**59.2207**	

Note:

1. Sample (bolded) represents body weight that is not significantly different in *star*$^{+/+}$ and *star*$^{-/-}$ fish. Their average body weight was 0.2473±0.01729 g and 0.2640±0.01149 g, and the statistical test *P*-value was 0.0761, which represents that body weight was not significantly different from each other. The average protein content in *star*$^{+/+}$ and *star*$^{-/-}$ fish was 55.99±2.578% and 59.80±2.601%, respectively, and the statistical test *P*-value was 0.0290 (*).

2. *: represents the significance of the difference in whole-body protein content of *star*$^{+/+}$ fish and body weight-matched *star*$^{-/-}$ fish.

Uncorrected Proof

Supplementary Table S4. List of overlapping DEGs in *star*, *cyp17a2* and *gr* knockout fish compared to their control siblings

Differentiated -expressed	Gene name	*star*$^{-/-}$ vs *star*$^{+/+}$ $\log_2$fold change	*cyp17a2*$^{-/-}$ vs *cyp17a2*$^{+/+}$ $\log_2$fold change	*gr*$^{-/-}$ vs *gr*$^{+/+}$ $\log_2$fold change
Down-regulated	*ugt5a2*	-6.427	-5.428	-9.544
	ddit4	-6.396	-6.176	-8.299
	fabp7a	-5.767	-3.430	-3.587
	zbtb16a	-5.380	-3.285	-3.813
	grik1a	-5.116	-2.024	-8.569
	fkbp5	-4.848	-4.968	-7.246
	si:ch211-152c8.5	-4.626	-2.826	-3.091
	nceh1a	-4.600	-4.070	-4.761
	desi1a	-4.064	-2.361	-4.033
	mtnr1al	-3.952	-4.640	-6.811
	hsd17b3	-3.904	-5.453	-7.222
	klf13	-3.888	-2.418	-3.771
	ugt5a1	-3.861	-4.234	-6.965
	igsf9ba	-3.728	-4.223	-4.663
	pacs2	-3.679	-3.448	-5.254
	hsd11b2	-3.644	-2.054	-4.376
	slc47a4	-3.636	-3.769	-2.834
	slc29a4	-3.449	-3.035	-2.497
	slc16a4	-3.374	-2.830	-2.37
	ascc1	-3.352	-2.129	-3.04
	tmem131	-3.131	-2.402	-3.166
	sephs1	-3.088	-2.582	-4.285
	tfcp2l1	-3.070	-2.772	-4.379
	arl5c	-3.042	-2.732	-4.259
	mkxa	-2.937	-4.713	-7.791
	tmcc1	-2.914	-3.806	-6.912
	apof	-2.896	-3.442	-5.096
	si:ch211-208k15.1	-2.735	-3.206	-4.462
	p4ha3	-2.626	-3.030	-2.32
	abcf2a	-2.625	-2.859	-3.22
	or131-2	-2.551	-4.571	-3.666
	zbtb16b	-2.538	-2.935	-2.364
	si:dkey-19b23.8	-2.522	-3.851	-3.257
	mafb	-2.511	-3.383	-4.379
	ifrd1	-2.461	-2.308	-3.391
	chrne	-2.451	-3.078	-4.531

uncorrected proof

	phkg1a	-2.341	-2.732	-7.282
	si:dkey-33i11.1	-2.267	-2.038	-2.186
	cpt1b	-2.188	-5.082	-4.846
	mybphb	-2.159	-3.984	-3.293
	si:ch211-210g13.5	-2.045	-3.001	-5.943
Up-regulated	*sult3st2*	2.248	2.503	4.3693
	slco1c1	2.562	2.985	8.635
	rnd2	2.889	3.679	4.5852
	trim9	2.899	2.615	2.4578
	il7r	3.187	3.265	3.3904
	cyp24a1	3.246	3.692	5.4404
	mdga2a	3.797	2.156	4.6555
	si:ch211-266c8.1	4.013	3.278	2.0182
	cyp7a1	4.771	2.020	6.7633
	hmgcra	5.447	5.392	2.6945
	mcm10	5.922	5.669	3.7361

uncorrected proof

斑马鱼的糖皮质激素信号通过调节肉碱棕榈酰转移酶 1b（*cpt1b*）转录进而促进脂肪酸 β-氧化（FAO）

张雨晴[1,2]，石生持[1,2]，李西[4,*]，石闯[1,2,3]，王馨怡[1,2]，许金丽[1,2]，娄气永[1,2]，金霞[1]，贺江燕[1]，殷战[7,6,1,2,5]，翟刚[1,2,5,7,*]

1 中国科学院水生生物研究所，水产品种创制与高效养殖全国重点实验室，湖北武汉 430072，中国

2 中国科学院大学，北京 100049，中国

3 海南大学，海洋生物与水产学院，南繁与热带高效农业协同创新中心，海南省水产种业工程研究中心，南繁学院，海南海口 570228，中国

4 温州医科大学附属康宁医院，临床研究中心，浙江温州 325035，中国

5 华中农业大学，湖北洪山实验室，湖北武汉 430070，中国

6 中国海洋大学，海水养殖教育部重点实验室，山东青岛 266003，中国

7 中国海洋大学深圳研究院，广东深圳 518100，中国

Uncorrected proof

摘要

脊椎动物糖皮质激素受体（Gr）介导的糖皮质激素（GC）信号对营养代谢至关重要，但该信号在脂质分解代谢中的作用和分子机制仍不清晰。本研究利用三种皮质醇合成不足模型（*pomca*$^{-/-}$、*star*$^{-/-}$和 *cyp17a2*$^{-/-}$斑马鱼）和一种糖皮质激素抵抗模型（*gr*$^{-/-}$斑马鱼），探究了 GC 信号在硬骨鱼类脂质代谢中的作用。我们在 *star*$^{-/-}$、*cyp17a2*$^{-/-}$和 *gr*$^{-/-}$斑马鱼中，均观察到了全身性能量代谢稳态重塑的特征，包括：脂肪沉积和葡萄糖利用增强。转录组结果显示，与各自对照同胞相比，在肝脏的差异表达基因中，下调的肉碱棕榈酰转移酶 1b（*cpt1b*）被鉴定为 *star*$^{-/-}$、*cyp17a2*$^{-/-}$和 *gr*$^{-/-}$斑马鱼三者所共有。机制上，使用氢化可的松（HC）处理可恢复 *star*$^{-/-}$和 *cyp17a2*$^{-/-}$斑马鱼的脂肪酸 β-氧化（FAO）能力，并挽救其肝脏和肌肉中下调的 *cpt1b* 表达，但在 *gr*$^{-/-}$斑马鱼中无效。进一步发现，GC 可通过 Gr 作用于 *cpt1b* 的近端启动子区域来激活其表达。通过比较四种缺陷模型相对于各自对照同胞血浆中激素水平的变化倍数时，发现 *pomca*$^{-/-}$斑马鱼的睾酮水平相对增幅最大，皮质醇水平和 *cpt1b* 表达量

相对降幅最小。因此，与其他三种 GC 信号受损的斑马鱼模型不同，*pomca*$^{-/-}$斑马鱼未观察到肥胖的现象。本研究表明，GC 信号通过促进 *cpt1b* 表达来增强 FAO，同时，GC 信号受损是否会导致肥胖，则取决于鱼类血浆中类固醇激素谱的综合影响。

关键词：糖皮质激素信号；脂肪酸 β-氧化；*cpt1b*；代谢重塑；类固醇谱

uncorrected proof